University of Mississippi

eGrove

1-1-2021

CONVECTIVE HEAT TRANSFER ENHANCEMENT OF A CHANNEL-FLOW USING HORIZONTALLY-ORIENTED PIEZOELECTRIC FANS

Janak Tiwari
University of Mississippi

Follow this and additional works at: https://egrove.olemiss.edu/etd

Part of the Mechanical Engineering Commons

CONVECTIVE HEAT TRANSFER ENHANCEMENT OF A CHANNEL-FLOW USING

HORIZONTALLY-ORIENTED PIEZOELECTRIC FANS

A Thesis

presented in the partial fulfillment of requirements

for the degree of MS in Engineering Science

in the Department of Mechanical Engineering

The University of Mississippi

by

Janak Tiwari

May 2021

ABSTRACT

Experimental and numerical studies were carried out to investigate the convection heat transfer enhancement of air channel flow using a piezoelectric fan, operated at 90.3 Hz. Its peak-to-peak displacement was increased up to 11.8 mm. The average velocity of channel flow was ranged up to 3 m/s, covering both laminar and turbulent flow regimes. The effects of fan location on the heat transfer performance were evaluated by changing the relative position of the fan tip to the heated surface. A maximum heat transfer enhancement of 102 % was obtained at the channel flow rate of 15 LPM. The fan was placed at the front-end location of the heated surface and operated with a displacement of 11.8 mm. For a fixed channel flow condition, the piezoelectric fan was found to improve the heat transfer performance only when operated with displacements larger than the critical value. The overall heat transfer performance of the heated surface in the channel was found to be dependent on the channel volume flow rate and the amplitude and frequency of the piezoelectric fan. The numerical study was performed using ANSYS Fluent to investigate complex flow fields created by the piezoelectric fan and their impact on the thermal responses of the heated surface in the channel. The Q-criterion analysis was used to identify vortical structures generated from the piezoelectric fan and understand their transport characteristics. It was found that the formation, propagation, and impinging dynamics of vortical structures were the significant factors that affected the convective heat transfer rate of the heated surface in the channel.

DEDICATION

This thesis is dedicated to all teachers who have blessed me with knowledge and wisdom.

LIST OF SYMBOLS

Nomenclature

A_c	Cross-section area of the channel (m^2)
A_{cu}	Cross-section area of the copper coupon (m^2)
C	Specific heat of the air (J / kg K)
D	Peak-to-peak amplitude of PE fan (mm)
d_{cf}	Hydraulic diameter of channel (m)
D_p	Mean to peak amplitude of PE fan (m)
E	Energy
f	Frequency of PE fan (Hz)
h	Heat transfer coefficient (W / m^2 K)
h_{cf}	Heat transfer coefficient measured only with channel flow (W / m^2 K)
h_e	Enthalpy
l	Distance between heated surface and thermocouples (m)
l_c	Hydraulic diameter of the copper coupon (m)
L	Streamwise length of the copper coupon (m)
L_b	Length of nickel blade of PE fan (m)
L_p	Length of Piezoelectric ceramics patch (m)
L_{PE}	Effective length of PE fan $= L_p + L_b$ (m)
L_s	Length of PE fan support (m)
k_{cu}	Thermal conductivity of copper (W / m K)
k_{air}	Thermal conductivity of air (W / m K)
$\dot{m}$	Mass flow rate (kg/s)
n	weighting factor of PE fan

Nu	Nusselt number
p	Pressure (Pa)
Pr	Prandtl number
q	Heat transfer rate (W)
$\dot{Q}$	Volume flow rate of channel flow (m³/s)
R^2	Coefficient of determination (r-squared)
Re_{cf}	Reynolds number of channel flow, $Re_{cf} = \dfrac{U_{cf} \cdot d_{cf}}{v_{air}}$
Re_{pf}	Reynolds number of PE fan, $Re_{pf} = \dfrac{U_{pf} \cdot W_p}{v_{air}}$
Re_{tot}	Total Reynolds number, $Re_{tot} = \sqrt{Re_{cf}^2 + nRe_{pf}^2}$
S	Distance between the tip of PE fan and rear end of heated surface (m)
St	Strouhal number, $St = \dfrac{U_{pf}}{\pi\,U_{cf}} = \dfrac{2fD_p}{U_{cf}}$
St_{cr}	Critical Strouhal number
t	Time (s)
T_{in}	Air inlet temperature (K)
ΔT_{LMTD}	Log mean temperature difference (K)
T_{out}	Air outlet temperature (K)
$T_{Sub,i}$	Temperature measured inside the copper block (K)
$T_{Surface,i}$	Temperature of the copper coupon (K)
U	Channel average velocity (m/s)
U_{cf}	Average velocity of the channel flow (m/s), $U_{cf} = \dfrac{\dot{Q}}{A_c}$
U_{in}	Velocity of the channel flow given at inlet in numerical study (m/s)
U_{pf}	Characteristic velocity of PE fan (m/s), $U_{pf} = 2\pi fD_p$

$\vec{v}$	Velocity vector
W	Width of the channel (mm)
W_p	Width of the PE fan (m)
y_{tip}	Trajectory of PE fan tip (m)
$y(\gamma,t)$	Displacement of PE fan at length γ and time t

Greek Symbols

ε	Effectiveness of PE fan, $\varepsilon = \dfrac{h}{h_{cf}}$
v_{air}	Kinematic viscosity of air (m^2/s)
ρ	Density
$\bar{\tau}$	Stress Tensor
ϕ	Phase angle

Abbreviations

PE fan	Piezoelectric fan
PTA	Piezoelectric Translational Agitator
PZT	Lead Zirconate Titanate
UDF	User Defined Function
VS	Vortical Structure

ACKNOWLEDGMENTS

I would like to thank my parents for their love and support throughout my life. My brother and sisters also deserve huge thanks. I would like to express my sincere appreciation and gratitude to my advisor, Dr. Taiho Yeom, for his guidance and support, not only regarding the academic counseling but also in making me acquainted to the social and cultural aspects of United States. I would also like to thank Dr. Tyrus McCarty and Dr. Wen Wu for serving on my committee.

Special thanks to all my friends and OleMiss family, who have supported me throughout the process. I will always appreciate all they have done to make my stay at OleMiss pleasant and exciting. Finally, I extend my thanks to all those unnamed individuals who helped me directly or indirectly for the accomplishment of my degree and this thesis.

TABLE OF CONTENTS

LIST OF FIGURES

LIST OF TABLES

CHAPTER 1

INTRODUCTION

Advancements in science and technology have created more powerful and compact electronic devices that dissipate a tremendous amount of heat. The safe and reliable operation of such devices needs efficient thermal management systems. Various thermal management techniques, such as liquid cooling, air cooling, direct sprays cooling, and multi-phase heat exchanger system, have been developed for satisfying the thermal management needs of power electronics. Although liquid cooling provides relatively high heat transfer capacity, a reliability issue associated with leakage is a big hurdle to overcome. Besides, they require complex supporting components, such as reservoir, pump, sprays, and nozzles, making them less attractive for electronics cooling applications. Therefore, air cooling remains one of the most attractive and efficient methods for the thermal management of electronics due to its simple configuration and high reliability. Natural convection cooling systems have a relatively low heat transfer capability. This makes them unsuitable for modern electronics that dissipate a large amount of heat. Thus, a forced convection cooling system is generally preferred. A rotary fan is one of the popular methods for creating a forced convection condition. However, the cooling performance of the rotary fan largely depends on its size and rotation speed, which has been limiting factors in its applications on complex and compact electronic devices. Thus, novel active cooling techniques(such as piezoelectric fan, twisting tape, synthetic jets) which can aid or replace a rotary fan, are of great interest.

1.1 Literature Review

A piezoelectric fan (PE fan) has been gaining attraction as an active cooling device. It is a thin, flexible metal or plastic cantilever plate (or blade) with either mono-morph or bi-morph patches of a piezoelectric material attached to the side surfaces. When an alternative current input signal at the resonance frequencies of the PE fan is provided on the piezoelectric patches, an amplified flapping motion is created at the tip of the blade. This flapping motion can be used to generate air currents for cooling heated objects or manipulating flow fields. Toda [1] carried out an experimental and theoretical investigation on airflows generated around vibrated cantilever beam. Yoo et al. [2] performed an experimental and theoretical analysis to understand the structural and dynamic characteristics of a PE fan with different configurations. They demonstrated that the resonant frequency of the PE fan is inversely proportional to the length of the fan. Acikalin et al. [3] found that the PE fan with a short blade and high operating frequency has a better cooling performance than a longer blade and low operating frequency. Wait et al. [4] studied the characteristics of airflows around a PE fan operating at higher resonance modes. According to the study, the power consumption of the PE fan increased significantly at the higher modes. Lei et al. [5] investigated the heat transfer performance of a PE fan with different resonant frequencies. The PE fan operating at the first resonant frequency was found to produce the best cooling performance among tested. Yoo et al. [2], Abdullah et al. [6], Liu et al. [7], and Lin et al.[8] concluded that the cooling performance of a PE fan is directly proportional to its amplitude. Kimber and Garimella [9] compared the impacts of amplitude and frequency on the cooling performance of a PE fan. The results indicated that the frequency was a more critical factor compared to the amplitude of the PE fan.

The cooling effect of a PE fan is known to largely depend on the flow dynamics created by its flapping motion. Various studies have been performed to understand the flow fields around PE fans. Many researchers [8–11] observed the formation of counter-rotating vortices near the vibrating blade of PE fan. Those vortices got fully developed when the PE fan blade reached the maximum amplitude and were finally detached from the fan tip [12,13]. The subsequent oscillation of the PE fan pushed the detached vortices downstream, and the cycle repeated. Using a phase-resolved particle image velocimetry (PIV) measurement, Kim et al. [14] studied the flow fields around a PE fan and captured a pair of counter-rotating vortices in each vibrating cycle. In their subsequent study using a phase-locked PIV measurement [15], they also identified vortical structures, which dominated the pseudo-jet flows around the PE fan. Agrawal et al.[16] used a two-dimensional phase-locked PIV to analyze the three-dimensional flow fields around PE fans and identified horse-shoe shaped vortical structures around them. They also obtained similar vortical structure in their numerical study.

Eastman et al. [17] analyzed two-dimensional flow fields around a PE fan in an enclosure and calculated the thrust generation. Eastman and Kimber [18] extended their study into the three-dimensional analysis and proposed the optimized geometry of the enclosure. Extending forward, Eastman and Kimber [19] measured aerodynamic damping effects caused on the sidewalls of the enclosure due to the dynamic operation of the PE fan. They found that, for the PE fan with small gaps from the sidewalls, the aerodynamic damping was about five times larger than that of the PE fan without the side walls. However, as the gap increased, the damping effects decreased and eventually became negligible at the gap of 10 mm. Sheu et al. [20] found that the amplitude of a PE fan had a linear relationship with the applied voltage when the effects of air damping were neglected. Oh et al. [21,22] conducted a three-dimensional numerical analysis on

the flow fields around a PE fan confined between two side walls. The three-dimensional flow field was mainly dominated by the interactions between the vortices created from the tip and side surfaces of the PE fan. The tip and side vortices were found to interact with each other creating much more complex secondary fluid structures. Especially, the propagation of side vortices was one of the critical factors in characterizing the flow fields with the PE fan.

Ma et al. [23] studied the cooling effect of a PE fan on a fin-type heat sink. They developed a linear correlation between the thermal and hydrodynamic performances. Huang et al. [24] performed numerical and experimental studies to find the optimum location of a PE fan in a vertical fin plate. The results indicated that the PE fan located at the center point of the fin plate provided the best heat transfer performance. Açikalin et al. [25] performed analytical, computational, and experimental investigations to understand the flow fields and cooling effects induced by PE fans. They developed a closed-form analytical streaming solution to conduct the numerical simulations for the PE fans. In the subsequent study, Açikalin et al. [26] found that the frequency offset from the desired operating frequency and the amplitude of the PE fans were two critical parameters affecting their cooling effects. The length of the PE fan and the distance between the PE fan and heat source were two other significant factors. Lin [8] conducted experimental and numerical studies to investigate three-dimensional thermal and flow fields generated by a PE fan. They reported significant heat transfer improvements (60 ~ 240% on the vertical arrangement and 80 ~ 260% on the horizontal arrangement) over the natural convection condition due to the operation of the PE fan. Abdullah et al. [27] performed a two-dimensional numerical study and PIV measurement to investigate the thermal and hydrodynamic performances of PE fans, which reduced the average temperature of a heat source by 68.9°C in their best arrangement and operating conditions.

No mechanical moving components [28], high energy efficiency [29–31], low noise level, and adaptability in small spaces [32] have made a PE fan a promising solution for thermal management of electronics. However, the cooling effects of PE fans are generally very localized, and this makes it challenging for them to replace rotary fans completely. Therefore, a PE fan can be considered as a supplemental component further to enhance the thermal performance of fan-assisted heat sink systems. Acikalin et al. [33] used a PE fan as an aid device to an axial fan for cooling a small laptop. The temperatures of the laptop decreased by more than 6°C due to the pure operation of the PE fan. Florio and Harney [34] investigated the thermal performance of a PE fan in a locally heated vertical channel under a natural convection condition. The PE fan improved the local heat transfer of the vertical channel by 52% compared to the base condition. Lin [35] performed three-dimensional flow visualizations and numerical simulations to study the cooling performance of a PE fan placed in the wake region of a cylinder in the presence of cross-flow. The PE fan improved the local and average heat transfer performance of the cylinder by 214% and 132%, respectively.

Li et al. [36] studied the effects of cross-flow on the cooling performance of the vertically oriented PE fan. The vortices formed by the PE fan were pushed downwards by the cross-flow. The averaged heat transfer coefficient of the combined system was increased by about 56% compared to pure PE fan operation. Li et al. [37] reported that the cross-flow significantly influenced the amplitude of the PE fan. The amplitude of the PE fan was reduced by up to 56% under the existence of cross-flow. They also reported that the PE fan was useful for improving the heat transfer performance only under the cross-flow with low velocities. The vortical streaming flow, induced by the PE fan, was suppressed and swept away due to the high momentum of cross-flow when its velocity was high. Jeng and Liu [38] experimentally studied

the impact of vertically oriented PE fans on the thermal and hydrodynamic performances of heat sink under the presence of axial flow. The results showed that the effectiveness of PE fan was high at low channel Reynolds numbers and slowly decreased as the channel Reynolds number increased.

Dey and Chakrborty [39] numerically studied the effect of an oscillating fin on disturbing the fully-developed boundary layers and enhancing the convection heat transfer. They developed the correlation between the Nusselt number, frequency, and amplitude of the oscillating fin. They also reported the existance the threshold frequency and amplitude of the PE fan above which the significant improvement in heat transfer could be achieved. The relative location of the PE fan had a minimal impact on thermal performance. The flow physics around the PE fan, aligned along a channel-flow, was studied numerically by Park et al. [40]. It was found that the flow velocity immediately downstream of the PE fan was increased significantly when the channel-flow velocity was low. However, the PE fan and the holding block acted as obstacles, decreasing the flow velocity downstream of the PE fan under the channel-flow with high velocities.

1.2 Motivation

As reviewed previously, extensive studies have been performed to understand the flow and thermal fields around PE fans at ambient conditions. Only a few studies have investigated the fluid dynamic and thermal effects of PE fans under the influences of existing flows. However, many unknowns are remained to fully uncover the related fluid and thermal phenomena around PE fans, especially for improving channel-flow convection heat transfer. The present study attempts explicitly to understand the enhancement of channel convection heat transfer using the PE fan, horizontally aligned along the direction of the channel flow. Experimental and numerical methods are used to achieve the objectives of the study.

6

CHAPTER 2

EXPERIMENTAL STUDY

2.1   Experimental Set-up
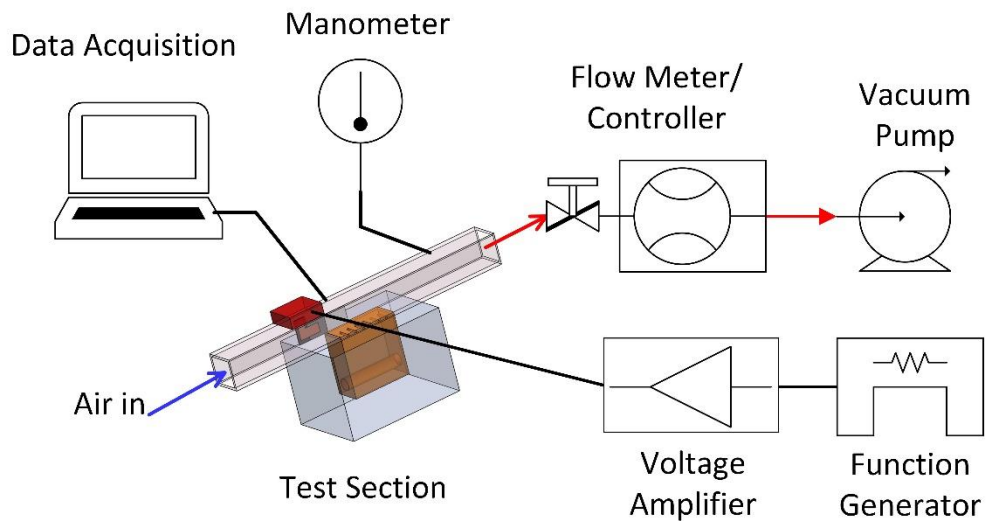
Figure 1. Schematic diagram of the heat transfer experimental set-up

Figure 1 shows the schematic diagram of the heat transfer experimental set-up of the

current study. The test section included a channel with a square cross-section of 22.3 mm × 22.3

mm. A copper coupon, used as a heated surface, was placed in the middle of a channel on the

bottom surface. Airflow was created by an external vacuum pump. The volume flow rate of the

channel flow was measured downstream of the channel using the Omega FMA-A2323 flow

meter, which has a measurement capability of 0-100 LPM. The pressure drop through the

channel was measured by the digital manometer, UEI EM 201B, which has a resolution of 0.1

Pa. Thermocouples were used to measure the channel inlet, outlet, and heated surface

temperatures. The EX-zone ST controller system from Watlow was used for data acquisition and analysis. The channel had adiabatic extensions at the upstream and downstream of the heated surface to make the flow nearly fully developed before entering the heated section. The channel had a specially designed slot in the top surface through which the PE fan assembly was installed. An alternating current signal from the Tektronix AGF-1062 function generator was amplified through the VF-500 linear piezoelectric amplifier (Dynamic Structures & Materials, LLC) and sent to the PE fan.
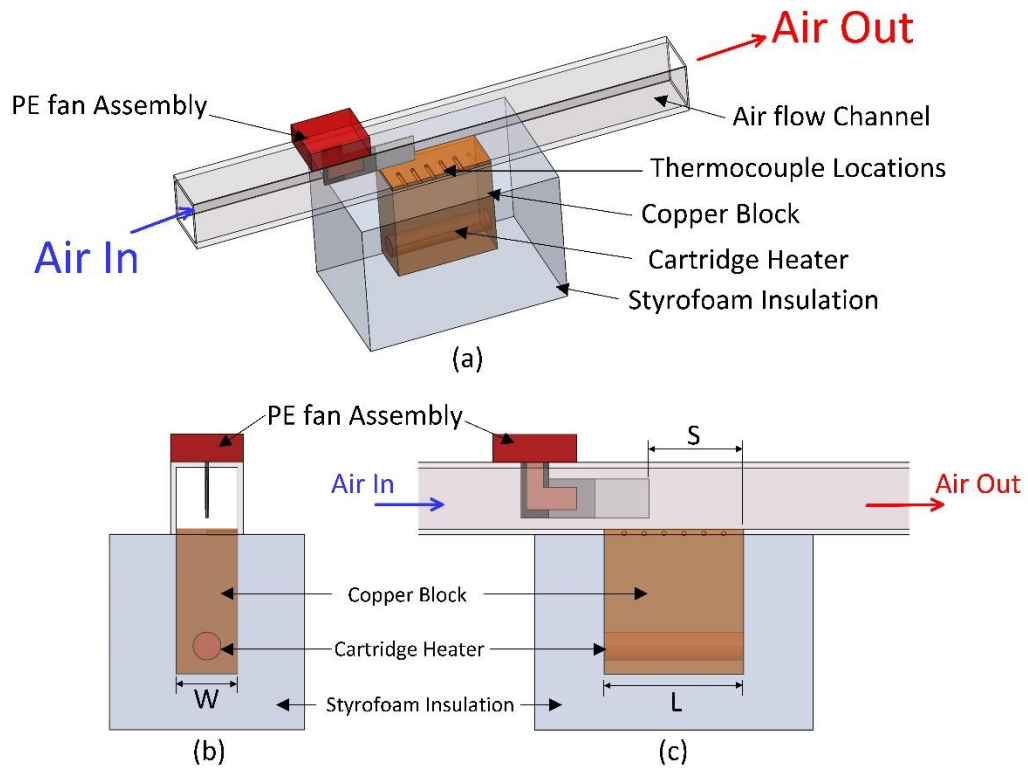
Figure 2. Detailed schematic of the test section (a) isometric view, (b) front view, (c) side view

The detailed schematic of the test section is illustrated in **Fig. 2**. A copper block was used to carry heat from a cartridge heater to the copper coupon, which has an area of 52 mm × 22 mm

and a thickness of 1 mm. The coupon was attached to the copper block using a thermal paste to reduce the thermal contact resistance. The channel was formed along the copper coupon to locate the heated surface in the middle of the channel. The remained surfaces of the copper block were completely insulated with Styrofoam to prevent any unnecessary heat loss. The PE fan was oriented along the streamwise direction while keeping the oscillation axis perpendicular to the flow direction and heated surface, as shown in **Fig. 2**. The tip of the PE fan faced the outlet of the channel. Therefore, air currents generated by the PE fan impinge in the same direction as the channel flow. The PE fan was centered in the channel along the vertical direction, leaving a gap of 4.15 mm from the channel bottom and top surfaces. A specially designed mount block, that could slide along the outer surfaces of the channel, was fabricated to install the PE fan in the channel. Therefore, the relative location of the PE fan could be adjusted along the streamwise direction without disassembling the entire channel system.
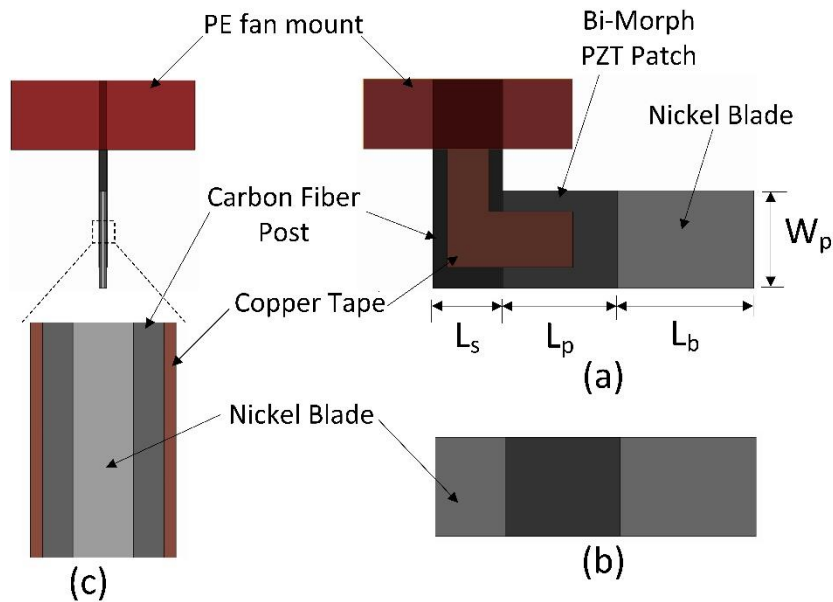
Figure 3. Configurations of Piezoelectric (PE) fan assembly. (a) PE fan assembled with carbon fiber post and copper tape, (b) Piezo bender actuator, (c) side view of PE fan assembly

9

Figure 3 shows the schematic of the PE fan used in the current study. A Lead Zirconate Titanate (PZT) bender actuator (**Fig. 3(b)**) was custom-designed. The bimorph-PZT patches sandwiched a flexible nickel blade in the center, leaving the extensions on both sides. One side of the nickel extension was used as a blade to generate air currents. The other side of the extension was used to attach a carbon fiber post (shown in **Fig. 3(c)**), fixed to the mounting block. An adhesive copper tape was used to make electrical connections from the PZT patches to the function generator. The thicknesses of the nickel blade and PZT patch were 0.05 mm and 0.2 mm, respectively. The thickness of the carbon fiber post in its assembled condition was 1.8 mm. The detailed dimensions of the PE fan are listed in **Table 1.**

Table 1. Dimensions of a PE fan

L_s (mm)	L_p (mm)	L_b (mm)	W_p (mm)
10	16.5	20	14

The entire channel and the PE fan assembly were sealed with silicon paste to prevent potential air leakage. The operating frequency of the PE fan was 90.3 Hz, which was the first resonance frequency. The flapping amplitude of the PE fan was obtained using the Keyence Displacement Sensor (II-030 sensor head) with a resolution of 1 μm. Li et al. [36] noted that the damping effects induced by the channel flow with low velocities had a negligible impact on the amplitude of the PE fan. Hence, in the current study, the amplitudes of the PE fan were characterized in the ambient condition. The trajectory of the fin tip, y_{tip}, for the PE fan is given as [36]:

$$y_{tip} = D_p \sin(2\pi f t) \qquad (1)$$

where D_p, f, and t are the mean-to-peak amplitude, frequency, and time, respectively. Then, the maximum fan tip velocity or the characteristic velocity, U_{pf}, of the PE fan is given as:

$$U_{pf} = 2\pi f D_p \qquad (2)$$

In the current study, the operating frequency of the PE fan was kept unchanged.

Therefore, the characteristic velocity of the PE fan was varied by changing the amplitude. **Table 2** summarizes the operating voltages and their corresponding mean-to-peak amplitudes and characteristic velocities of the PE fan. The average velocity of channel flow, U_{cf}, is obtained by dividing the volume flow rate ($\dot{Q}$) with the channel cross-section area (A_c) as:

$$U_{cf} = \frac{\dot{Q}}{A_c} \qquad (3)$$

Table 2. Operating Conditions of PE fan

Voltage (V)	0	40	60	80	120	170
Mean-to-peak Amplitude (mm)	0	0.65	2.05	3.50	4.75	5.90
Characteristic Velocity (m/s)	0	0.37	1.22	1.99	2.77	3.35

The Reynolds number (Re_{cf}) of channel flow is defined as:

$$Re_{cf} = \frac{U_{cf} \cdot d_{cf}}{\nu_{air}} \qquad (4)$$

where d_{cf} and ν_{air} are the hydraulic diameter of the channel and kinematic viscosity of air, respectively.

Table 3. Operating Conditions of Channel Flow and Corresponding Reynolds Numbers

Channel Flow Rate (LPM)	15	30	45	60	75	90
Channel Average Velocity (m/s)	0.5	1.0	1.5	2.0	2.5	3.0
Channel Reynolds Number	603	1205	1808	2410	3013	3616

Table 3 summarizes the volume flow rates of the channel and their corresponding average velocities and Re_{cf} used in the current study. The Reynolds number (Re_{pf}) of the PE fan is defined as:

$$Re_{pf} = \frac{U_{pf} \cdot W_p}{v_{air}} = \frac{2\pi f D_p \cdot W_p}{v_{air}} \qquad (5)$$

where W_p is the width of the PE fan.

2.2 Data Reduction

Two thermocouples were used to measure the inlet (T_{in}) and outlet (T_{out}) temperatures of the channel flow. Six thermocouples were embedded in the copper block at the locations 2 mm underneath the heated surface. The temperatures measured in the copper block are denoted as $T_{Sub,i}$. From these temperatures, the local surface temperatures of the heated surface, $T_{Surface,i}$ were extrapolated as:

$$T_{Surface,i} = T_{Sub,i} + \frac{q \cdot l}{k_{cu} \cdot A_{cu}} \qquad (6)$$

where q, l, k_{cu}, and A_{cu} represent the heat input from the heater, the distance between the thermocouples in the copper block and heated surface, the thermal conductivity of copper, and the cross-section area of the copper block, respectively. The average temperature of the heated surface, $T_{Surface}$, was achieved as:

$$T_{Surface} = \frac{\sum_{i=1}^{N} T_{Surface,i}}{N}, \quad N = 6 \qquad (7)$$

Using the energy balance between the inlet and outlet of the channel, the heat input to the channel was calculated as:

$$q = \dot{m}C(T_{out} - T_{in}) \qquad (8)$$

where $\dot{m}$ and C are the mass flow rate of the channel and specific heat of air, respectively. The average heat transfer coefficient (h) of the heated surface was calculated by the Log Mean Temperature Different method as:

$$h = \frac{q}{A_{cu}} \cdot \Delta T_{LMTD} \tag{9}$$

where ΔT_{LMTD} represent the log mean temperature difference which was computed by:

$$\Delta T_{LMTD} = \frac{\Delta T_2 - \Delta T_1}{ln(\Delta T_2/\Delta T_1)}$$

$$\Delta T_1 = T_{Surface} - T_{In}, \qquad \Delta T_2 = T_{Surface} - T_{Out} \tag{10}$$

where ΔT_1 and ΔT_2 denote the temperature differences between the heated surface and the inlet and outlet of the channel, respectively. Therefore, the average Nusselt number of the heated surface was calculated as:

$$Nu = \frac{hl_c}{k_{air}} \tag{11}$$

where k_{air} and l_c are the thermal conductivity of air and hydraulic diameter of the heated surface.

2.3   Data Validation and Uncertainty Analysis

In order to validate the experimental methodology utilized in the current study, the heat transfer of the heated surface, characterized without the operation of PE fan, was compared to the analytical relation of local Nusselt number for a flat surface with an unheated starting length and a constant wall temperature, given as [41]:

$$Nu_x = \frac{0.332 \, Re_x^{0.5} \, Pr^{\frac{1}{3}}}{\left[1 - \left(\frac{x_0}{x}\right)^{\frac{3}{4}}\right]^{\frac{1}{3}}} \tag{12}$$

where Nu_x, Re_x, Pr, and x_0 are the local Nusselt number, local Reynolds number, Prandtl number, and starting length of the heated surface, respectively. x represents a streamwise distance from the leading edge of the heated surface. Equation (12) is valid for $Re_x < 5 \times 10^5$ and $0.6 < Pr < 50$.

Then, the average Nusselt number of the heated surface was obtained by integrating the local

Nusselt number over the entire length of the heated surface.
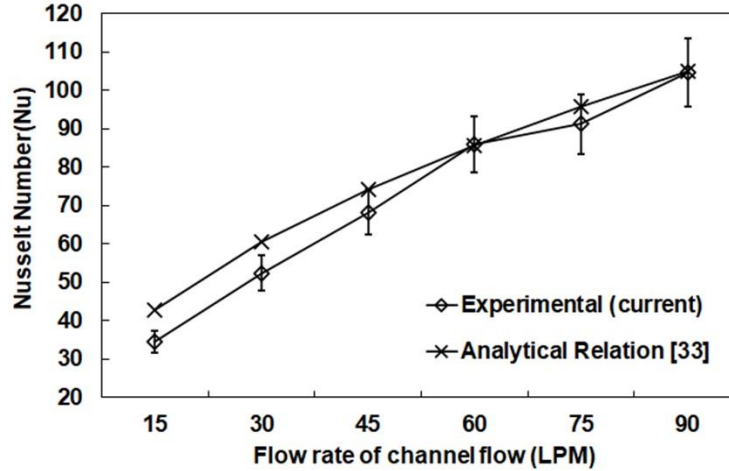
Figure 4. Comparison between experimental and empirical Nusselt Numbers for the baseline

condition

Fig. 4 shows the comparison between the experimental and analytical average Nusselt

numbers for the baseline condition that was tested without the operation of the PE fan. The

experimental data showed the deviations of approximately 20% from the analytical solution at 15

and 30 LPM, which fell in the laminar flow regime. However, the deviation started decreasing as

the flow entered the turbulent flow regime with the increased flow rate. At the flow rates higher

than 45 LPM, the deviations dropped to below 5 %. The total uncertainty in the experimental

heat transfer results was propagated from the uncertainties that existed in the measurements of

temperature and channel flow rate. The uncertainty analysis was performed to estimate the error

in the heat transfer results of the current study. The error in temperature reading was taken as ±

1%. The measurement error of the flow meter was taken as ± 1%. As a result, the total

uncertainty of the heat transfer coefficient was calculated as ± 8.5 %. The error bars, based on the

total uncertainty, were listed on the experimental data in Fig. 4. The deviations of more than 20

%, shown in the laminar flow regime, are statistically meaningful considering the total uncertainty of the heat transfer coefficient. However, the reason for the deviations was not yet evident in the current study. More investigations needs to be performed to close the deviations in the future studies.

2.4 Results and Discussions

2.4.1 Heat Transfer Coefficients

The heat transfer experiments were performed by locating the PE fan at three different relative locations from the heated surface in the channel. The three PE fan locations are denoted as the upstream, front-end, and center location, defined with the ratio of S/L, as shown in **Fig. 2**. S denotes the distance between the PE fan's tip and the trailing edge of the heated surface. L denotes the length of the heated surface. The values of S/L for the three different locations of PE fan are summarized in **Table 4**.

Table 4. Positions of PE Fan in the Channel

PE Fan Location	Upstream	Front-end	Center
S/L	1.5	1	0.5
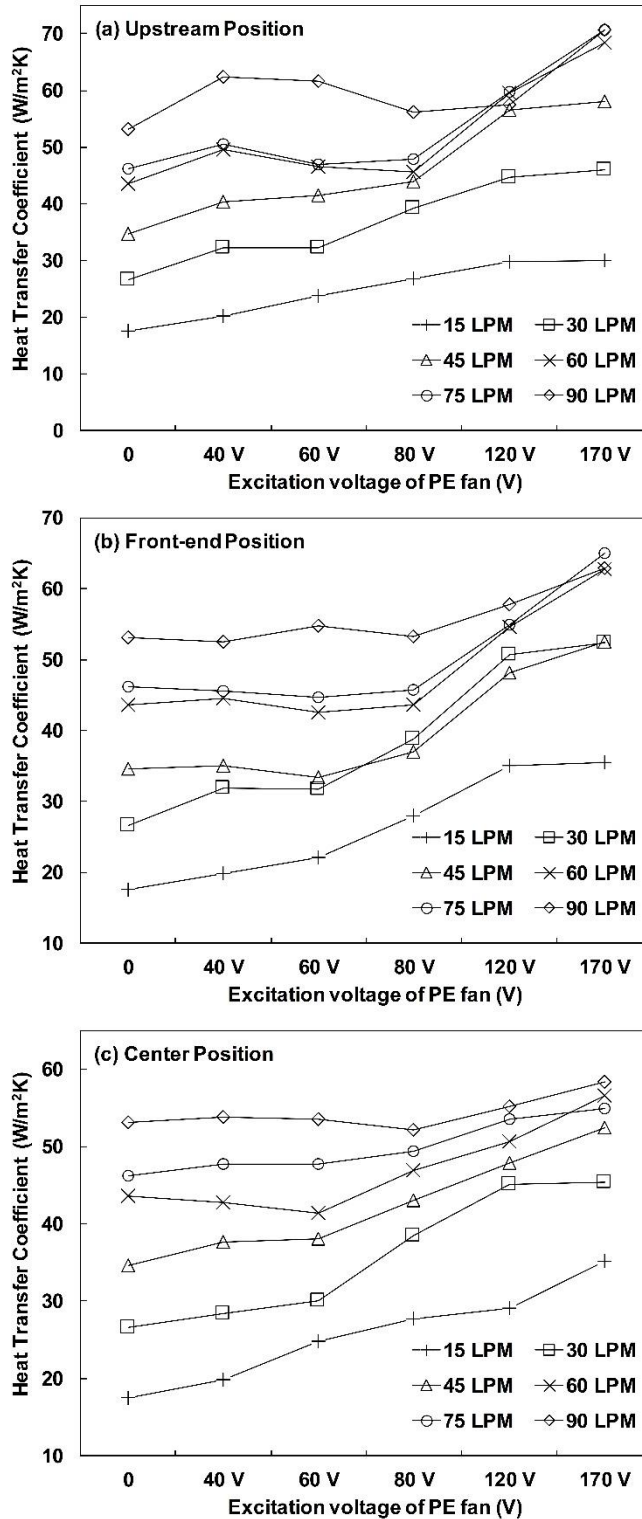
Figure 5. Heat transfer performance of PE fan with different excitation voltages: (a) PE fan at the upstream, (b) PE fan at the front-end, (c) PE fan at the center.
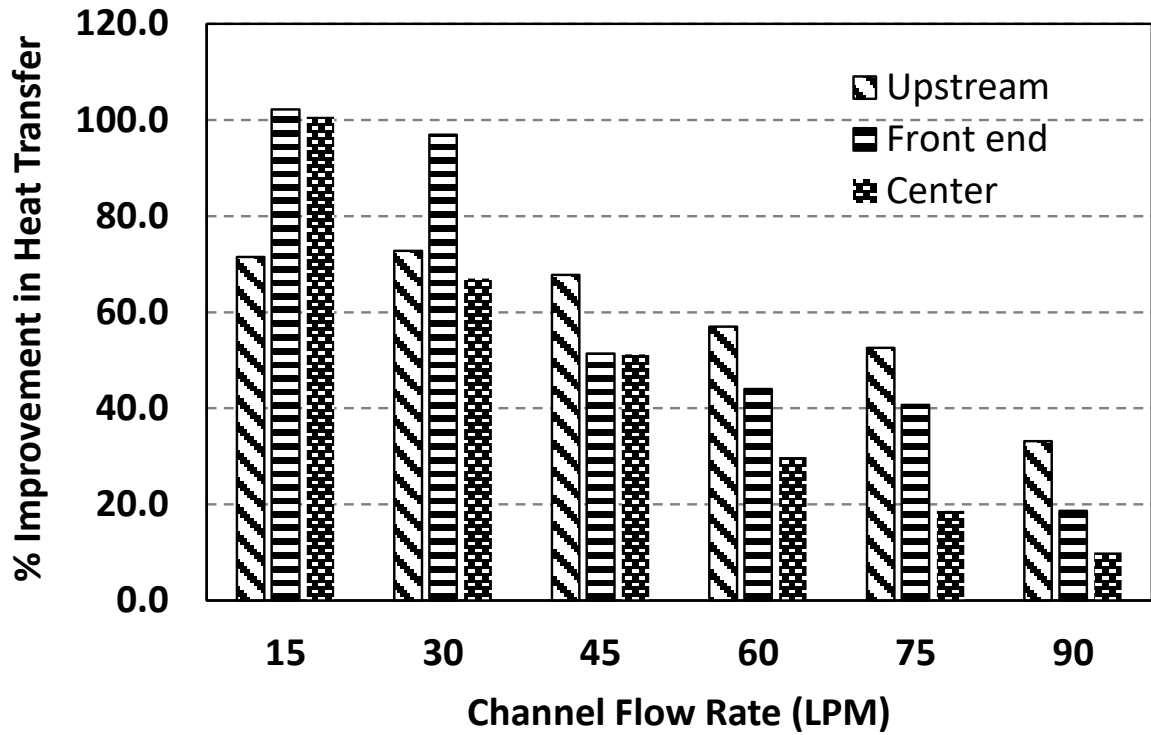
Figure 6. Percentage improvements in heat transfer coefficient of the heated surface with the PE fan at its maximum amplitude.
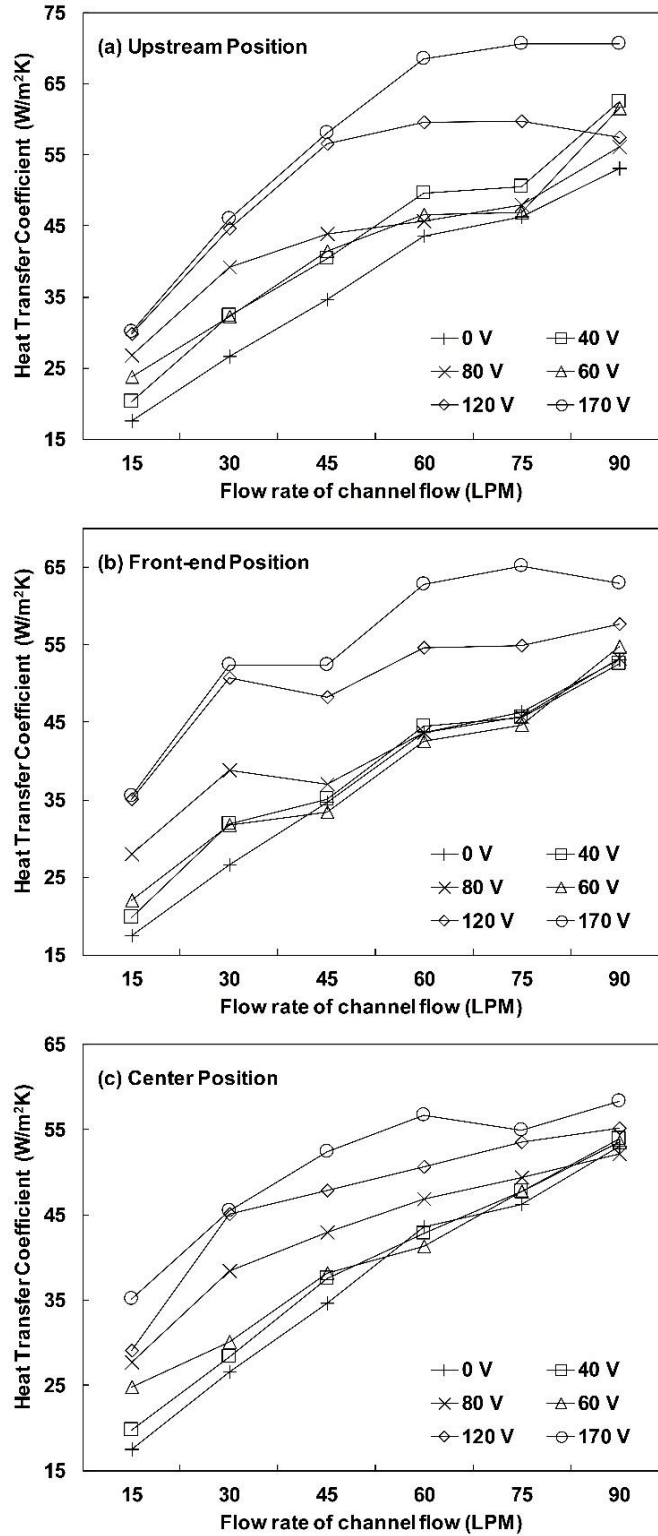
Figure 7. Heat transfer performance of PE fan with different channel flow rates: (a) PE fan at the upstream, (b) PE fan at the front-end, (c) PE fan at the center.
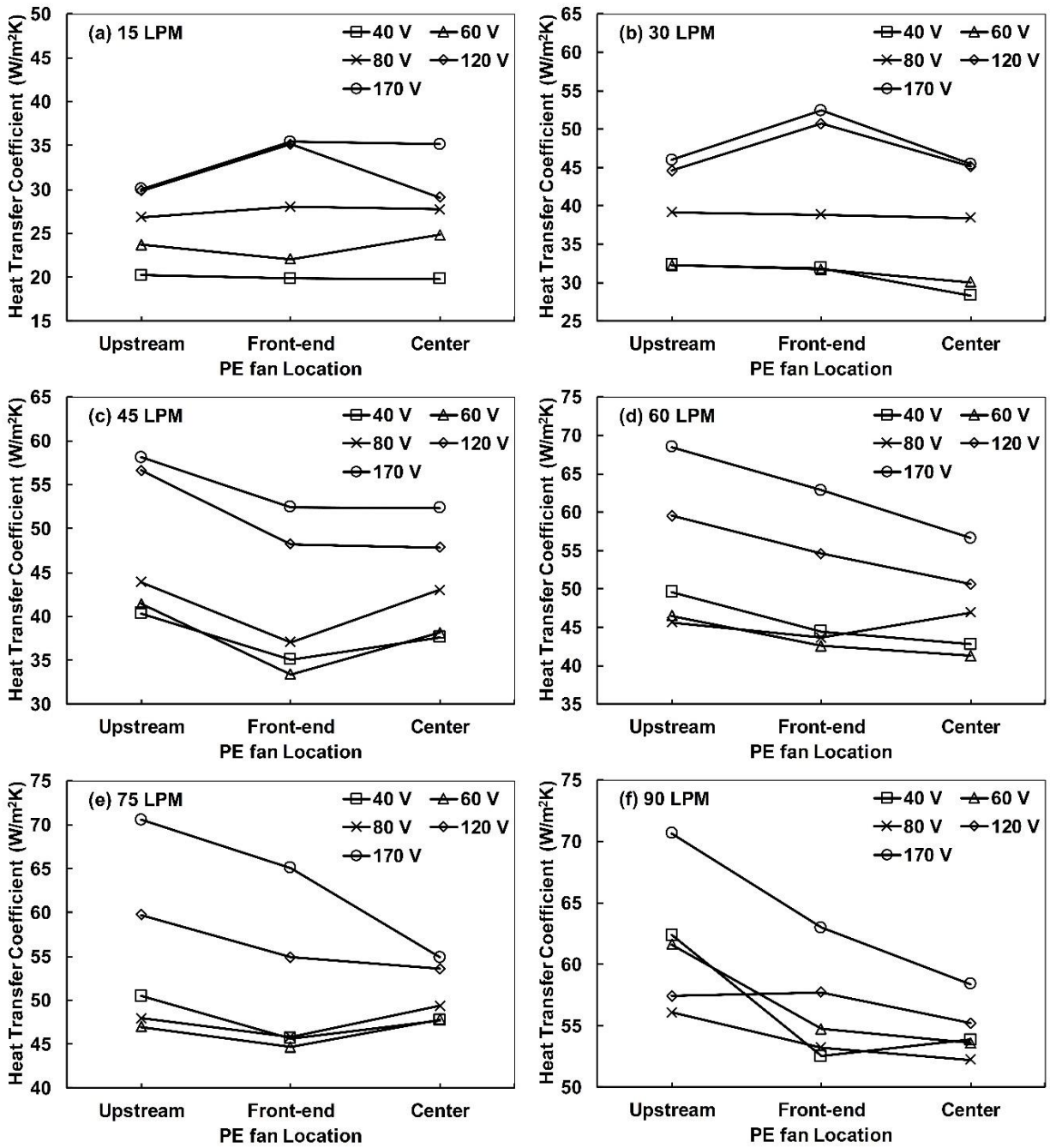
Figure 8. Heat transfer performance of the PE fan placed at different locations in the channel: (a) 15 LPM, (b) 30 LPM, (c) 45 LPM, (d) 60 LPM, (e) 75 LPM, (f) 90 LPM

Figures 5, **6, and 7** show the enhancements of the heat transfer coefficient achieved by the PE fan at the different applied voltages and channel flow rates. In **Fig. 5**, when the PE fan

19

was not operated, the baseline heat transfer coefficient of the heated surface increased from 17.5 to 53.0 W/m^2K while the channel flow rate was increased from 15 to 90 LPM. After the PE fan was turned on at the upstream location with its maximum excitation voltage of 170 V, the heat transfer coefficient of the heated surface increased 71.5% over the baseline condition at 15 LPM. At the largest flow rate of 90 LPM, the PE fan with the maximum amplitude enhanced the heat transfer coefficient by 33.2%. When the PE fan with the maximum amplitude moved to the front-end location, the heat transfer enhancements over the baseline condition were 102.2% and 18.7% for the flow rates of 15 and 90 LPM, respectively. This indicated that the PE fan was more effective at the front-end location in improving the heat transfer of the surface when the channel flow rate was low. On the other hand, at the higher channel flow rates, the PE fan was more effective at the upstream location. This trend continued when the PE fan was moved further downstream to the center location, generating the heat transfer improvement of only 10% at the flow rate of 90 LPM. The percentage improvements of the heat transfer coefficient by the PE fan, operating at its maximum amplitude for the entire range of channel flow rate, are shown in **Fig. 6**.

At the lower flow rates of 15 and 30 LPM, the heat transfer coefficient increased with an increase in the excitation voltage of the PE fan. On the other hand, at the higher flow rates of above 45 LPM, the heat transfer coefficient did not increase or even decrease until the excitation voltage exceeded 80 V. When the PE fan was excited with the voltages above 80 V, sudden increases in the heat transfer coefficient were observed. This stagnation or drop of heat transfer coefficient found at low excitation voltages and high channel flow rates was a clear pattern, which could be observed at all three locations of the PE fan. In **Fig. 7**, it was noticeable that the heat transfer rate decreased as the channel flow rate increased above 60 LPM, especially when

20

the PE fan was excited at the high voltages of 120 and 170 V. This may be hypothesized that induced complex flow motions from the PE fan and channel flow act against each other creating a net negative effect of decreasing heat transfer performance at the specific operating conditions. This phenomenon became even more evident when the PE fan was positioned at the upstream location.

Figure 8 shows the location effects of the PE fan on its heat transfer performance. While the heat transfer performance of the PE fan did not show robust linear patterns with respect to its location, some notable observations could be made. When the channel flow rate and excitation voltage were in their low ranges (15 ~ 30 LPM and 40 ~ 80 V), the location had a negligible impact on the heat transfer performance of the PE fan. Once the excitation voltage increased beyond 80 V on the same range of channel flow rate, the PE fan at the front-end location stood out in the heat transfer performance. This pattern changed as the channel flow rate further increased. At the channel flow rate of 45 LPM, the PE fan at the upstream location provided the superior heat transfer performance, whereas the PE fan at the front-end location showed the poorest performance. However, at the higher flow rates of 60, 70, and 95 LPM, the PE fan generally showed better heat transfer performance as it shifted further upstream from the heated surface. These trends agreed well with the observations made earlier from **Fig. 5**. The heat transfer performance patterns related to the PE fan's location may seem to be irregular. However, in general, the PE fan either at the upstream or front-end location provided a better heat transfer performance than the one positioned at the center location regardless of the channel flow rates tested. This is contrary to the general intuition that the PE fan may be superior in enhancing the heat transfer when it is more closely positioned to the heated surface due to its direct sweeping effects. Based on the observations made so far, two things can be hypothesized. First, the main

21

mechanisms of the heat transfer enhancement by the PE fan in the channel are stemming from

not only the direct sweeps of the flapping blade over the heated surface but also the agitations of

the flow caused by coherent vortical structures [40] created and transported from the PE fan.

Second, the interactions between these coherent vortical structures and the channel flow are

highly non-linear phenomena under the different conditions of PE fan's location and amplitude.

These may be the main causes of the irregular patterns in the heat transfer responses observed in

Figs. 5, 6, and 7. Eventually, high-level flow visualizations will be required to understand the

underlying mechanisms of heat transfer enhancement by the PE fan in the channel.

2.4.2   Effectiveness of PE fan

In order to characterize the relative contribution of the PE fan over the channel flow on

the total heat transfer of the channel flow, the effectiveness (ε) of the PE fan was defined as:

$$\varepsilon = \frac{h}{h_{cf}}$$
(13)

where h_{cf} is the heat transfer coefficient measured when only the channel flow is activated.

Again, h is the heat transfer coefficient of the heated surface measured when both the PE fan and

channel flow are activated. **Figure 9** shows ε of PE fan with respect to Re_{cf} at different excitation

voltages. In general, ε increased as the excitation voltage or the amplitude increased for almost

all the range of Re_{cf}. For the PE fan excited at the same voltage, ε decreased as Re_{cf} increased.

Regarding the location, the PE fan aligned at three different locations generally showed similar ε

when the excitation voltage was maintained below 80 V for the entire range of the channel flow

rate. On the other hand, as the excitation voltage increased above 80 V, the deviation in the ε

between the three locations started to be recognizable. When the channel flow was in the laminar

regime ($Re_{cf} < 2,000$), the PE fan at the front-end location was more effective in enhancing the

channel heat transfer than the other two locations. However, when the channel flow was in the turbulent regime ($Re_{cf} >$ 2,000), the PE fan at the upstream location was more effective. Overall, the channel flow provided more contribution on the total heat transfer enhancement than the PE fan as ε stayed below 2.0 for nearly all the ranges of parameters tested, with a few exceptions. At $Re_{cf} =$ 603, the PE fan (170 V) at the front-end and center locations made the contributions of slightly more than 50% on the total channel heat transfer with ε values of 2.02 and 2.01. These were the two locations where the PE fan provided direct sweeping contacts on the heated surface. This reflects that the PE fan's direct sweeping is one of the critical factors for improving the heat transfer of the heated surface in the channel. Moreover, from the observation that the PE fan at the upstream location provided better cooling performance when the channel velocity was high, it can be noted that the channel flow must be fast enough to carry the vortical structures created from the PE fan to the heated surface before they decay.
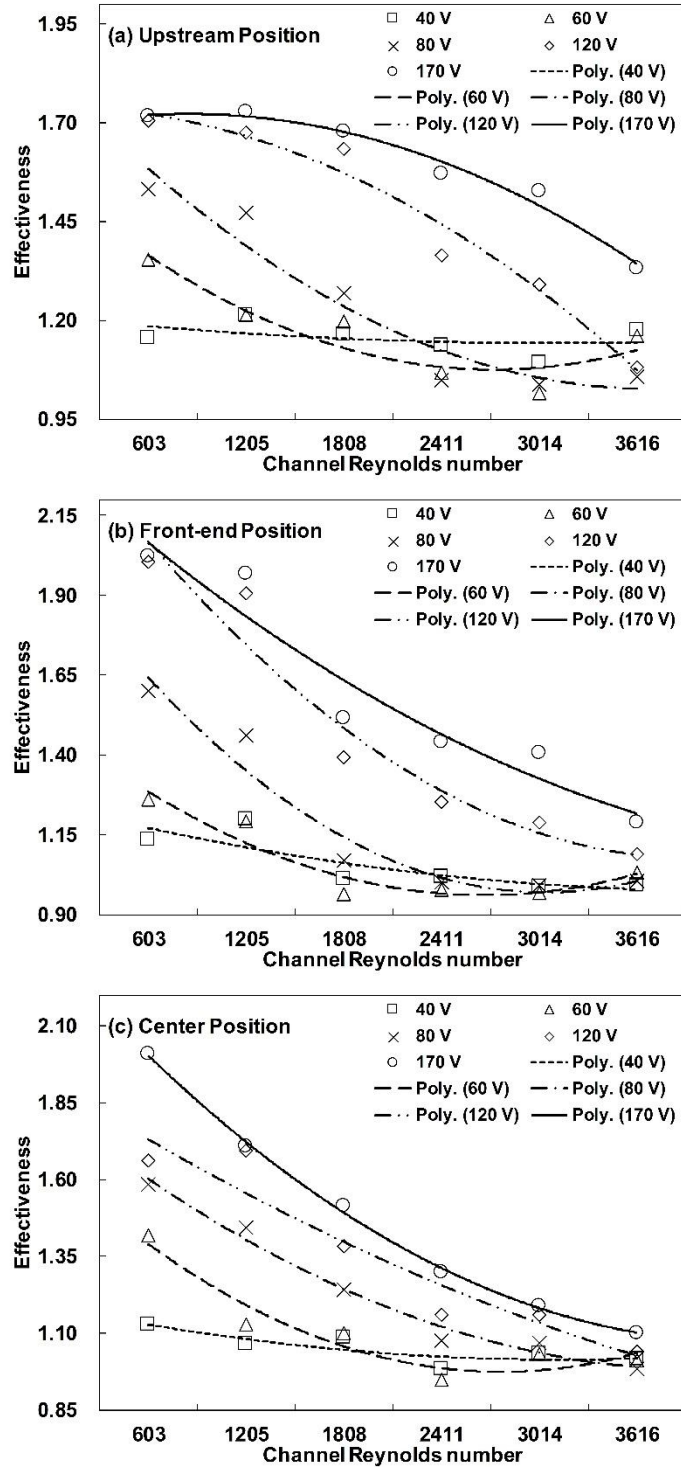
Figure 9. The relation between the effectiveness of PE fan and channel flow Reynolds number: (a) PE fan at the upstream, (b) PE fan at the front-end, (c) PE fan at the center.
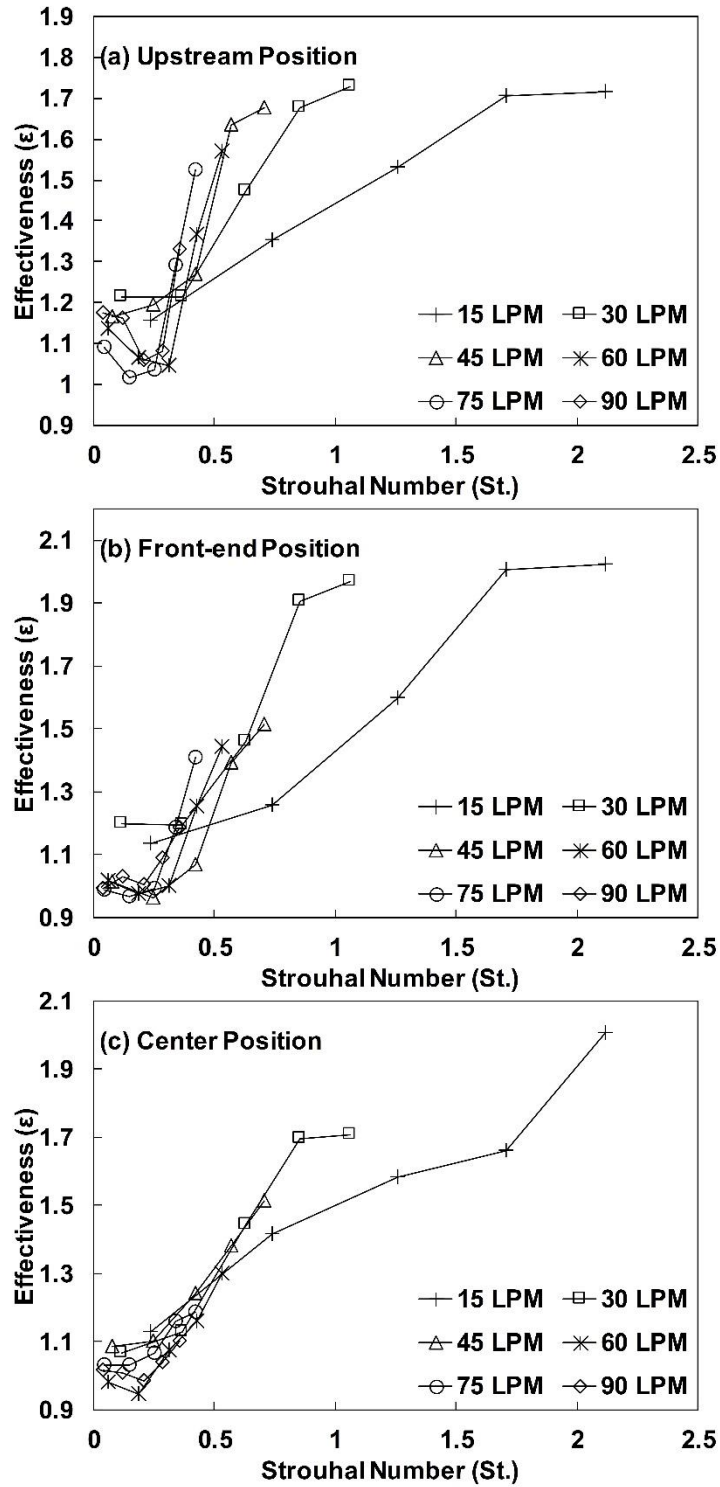
Figure 10. The relation between the effectiveness of PE fan and Strouhal number: (a) PE fan at the upstream, (b) PE fan at the front-end, (c) PE fan at the center.

The ratio of the characteristic velocity of the PE fan (U_{pf}) to the channel flow velocity (U_{cf}) becomes the Strouhal number (St) [40]:

$$St = \frac{U_{pf}}{\pi \, U_{cf}} = \frac{2fD_p}{U_{cf}} \qquad (14)$$

where f and D_p are the operating frequency and mean-to-peak amplitude of the fan. In the current study, the St measures the modulation of the channel flow caused by the operation of the PE fan. To better understand the effects of PE fan on the convection heat transfer of channel flow, ε of the PE fan was plotted against St for the three different locations under the full range of the channel flow rate, as shown in **Fig. 10**. There was one pronounced pattern found from the PE fan located at all three different locations. As St increased, ε tended to decrease, reaching its minimum values. It then increased again except for the cases with the channel flow rate of 15 LPM, where the ε continuously increased. In contrast, the St was kept increasing. This trend stood out under the larger channel flow rates of 60, 75, and 90 LPM. This indicates that the PE fan hinders the channel flow from enhancing the convective heat transfer of the heated surface until its amplitude reaches certain values under the specific conditions of flow rates. We can define St at these threshold amplitudes as the critical Strouhal number (St_{cr}), which lies around 0.2 for all the PE fan locations and channel flow rates tested in the current study. A similar finding was shown in the study by Park et al. [40]. The maximum axial velocity (spanwise velocity of the flow measured at a short distance from the fan tip along the streamwise direction) initially decreased and reached the minimum value at the threshold of $St = 0.13$. Then it increased again when $St > 0.13$. Their results indicated that the PE fan could add additional momentum to the channel flow only when the St exceeded 0.13.
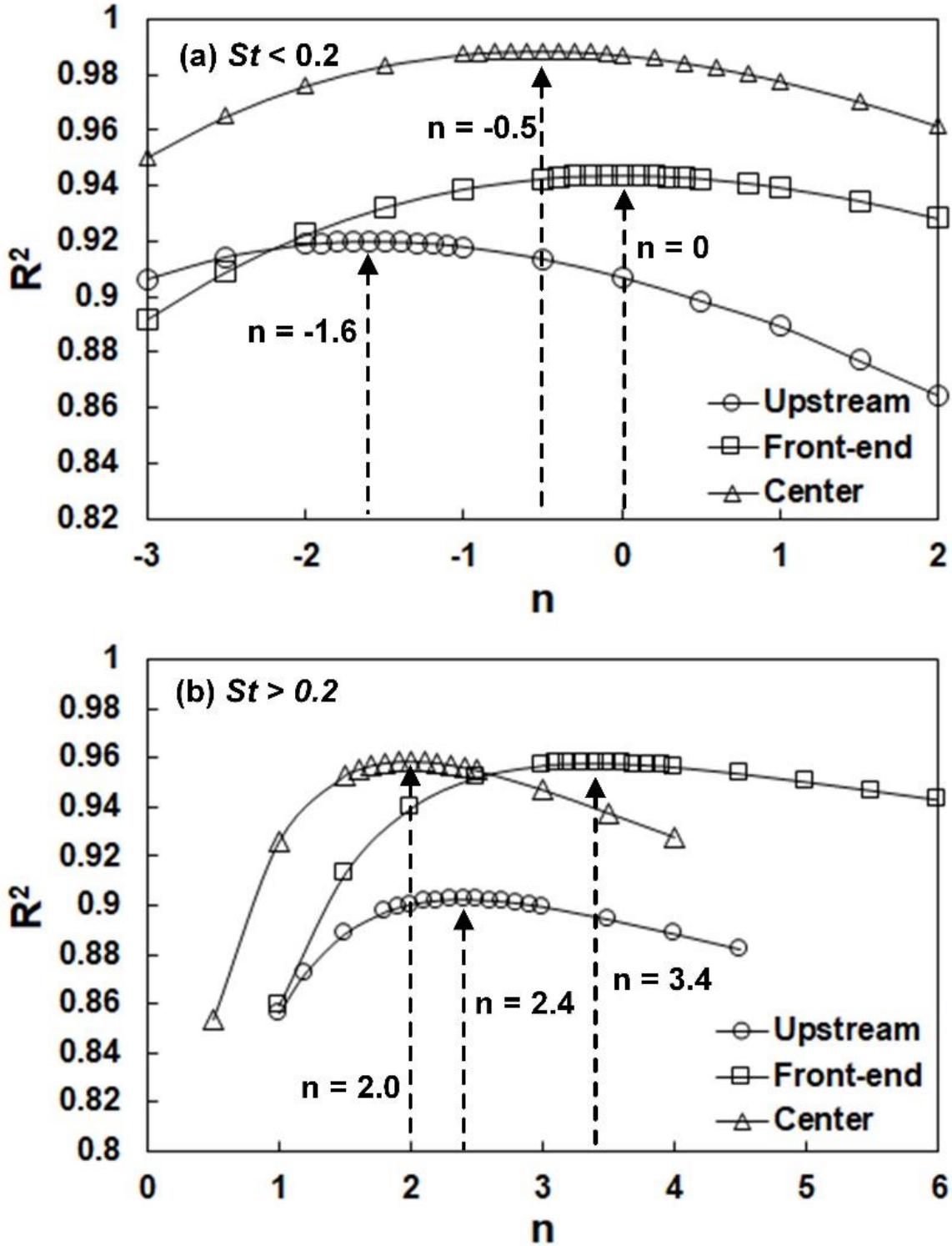
Figure 11. R-squared with respect to various weighting factors: (a) St < 0.2 and (b) St > 0.2.
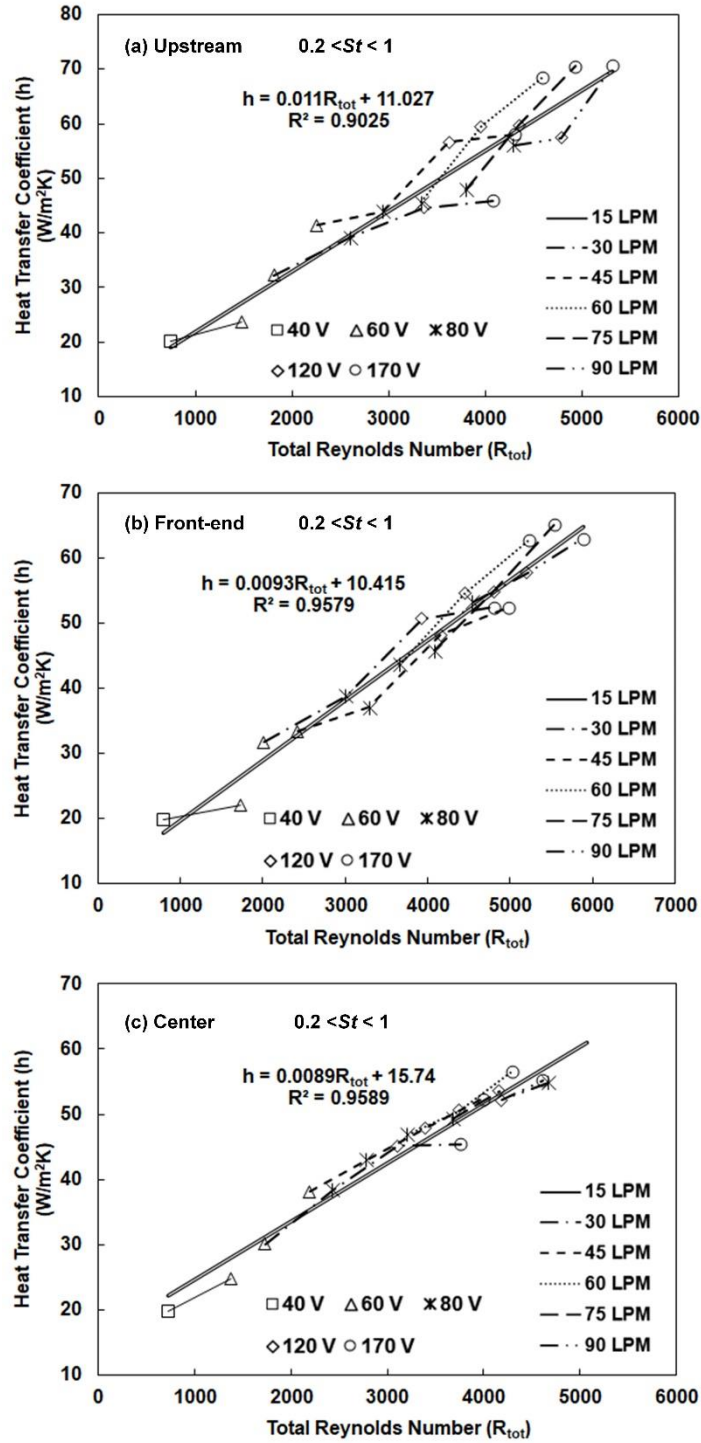
Figure 12. The relation between the heat transfer coefficient and total Reynolds number (for $St > 0.2$): (a) PE fan at the upstream, (b) PE fan at the front-end, (c) PE fan at the center.
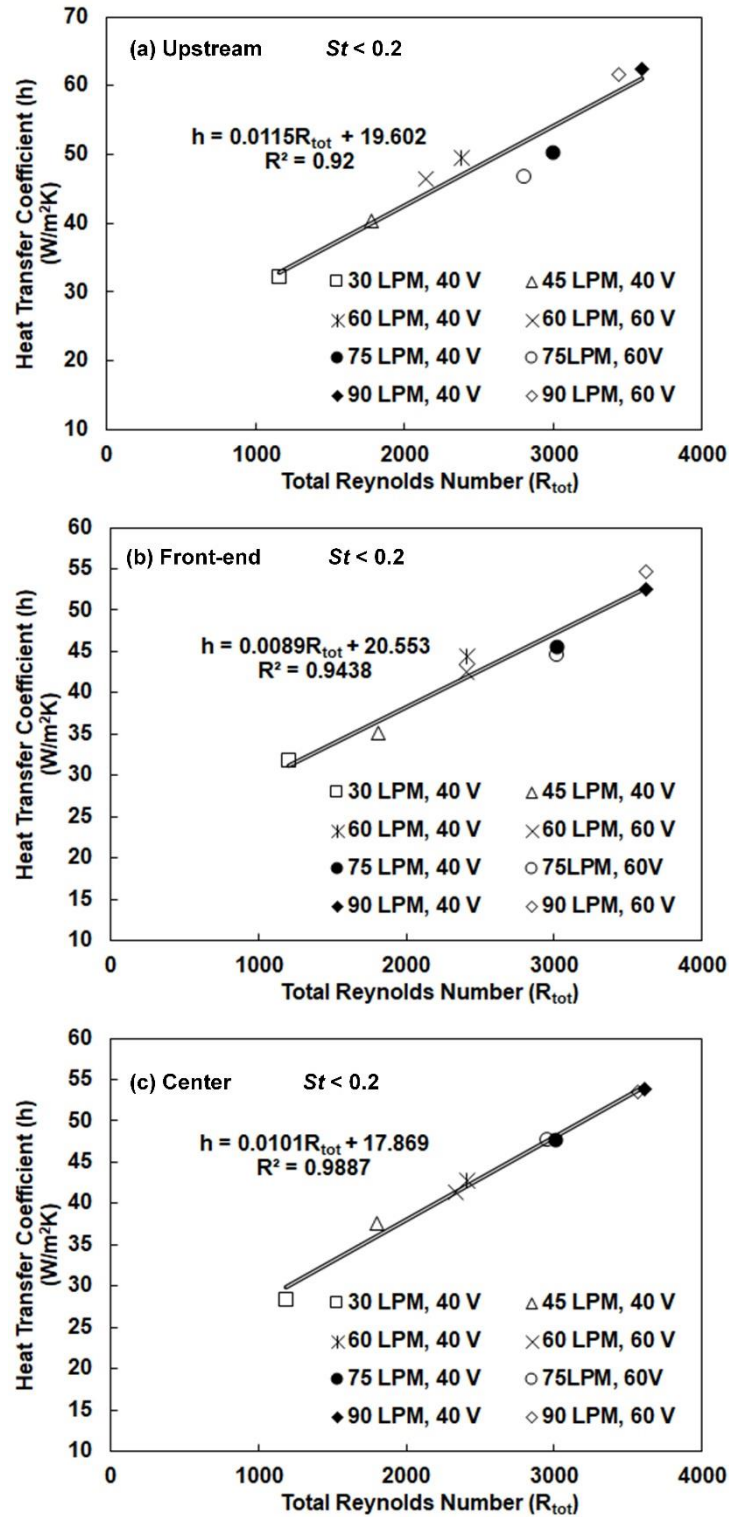
Figure 13. The relation between the heat transfer coefficient and total Reynolds number (for St < 0.2): (a) PE fan at the upstream, (b) PE fan at the front-end, (c) PE fan at the center.

In the current study, the total heat transfer of the channel can be characterized in terms of the combined effects of PE fan and channel flow by defining the total Reynolds number (Re_{tot}) as [42–44]:

$$Re_{tot} = \sqrt{Re_{cf}{}^2 + nRe_{pf}{}^2}$$

(15)

where n is the weighting factor that scales the effect of the PE fan against the channel flow. By substituting the original expressions of Re_{cf} and Re_{pf} (equations (4) and (5)) to equation (15), the total Reynolds number becomes:

$$Re_{tot} = \sqrt{\left(\frac{U_{cf} \cdot d_{cf}}{v_{air}}\right)^2 + n\left(\frac{2\pi f D_p \cdot W_p}{v_{air}}\right)^2}$$

(16)

In order to find the values of n that can provide the accurate correlations between the h and Re_{tot}, the coefficient of determination or r-squared (R^2) [45] of the correlations was examined while iterating different values of the n. Then, the values of n, which generated the maximum R^2, were selected to build the correlations for the PE fan at three different locations. This process was done separately for the cases of $St < 0.2$ and $St > 0.2$ (where $St_{cr} = 0.2$) since they showed the opposite characteristics in the heat transfer responses. **Figure 11** shows the calculations of R^2 with different values of n. For the cases of $St > 0.2$, the selected n values are 2.4, 3.4, and 2.0 for the upstream, front-end, and center locations, respectively. For the cases of $St < 0.2$, the selected n values are -1.6, 0, and -0.5 for the upstream, front-end, and center locations, respectively. The negative n values represent that the PE fan degrades the heat transfer performance of the channel for the given flow rate conditions. In contrast, $n = 0$ represents that the PE fan's contribution to the channel heat transfer is negligible. **Figures 12 and 13** show the relationships between the h and Re_{tot} for different experimental conditions and St. The correlations were made with the n

30

values identified earlier from the maximum R^2 values. Overall, h was found to have linear relation with Re_{tot} regardless of the St ranges. These correlations could be used to estimate the heat transfer performance of the PE fan in the channel flow for the given operating conditions of frequency, amplitude, channel flow rate, and PE fan's relative location.

2.4.3 Pressure Drop
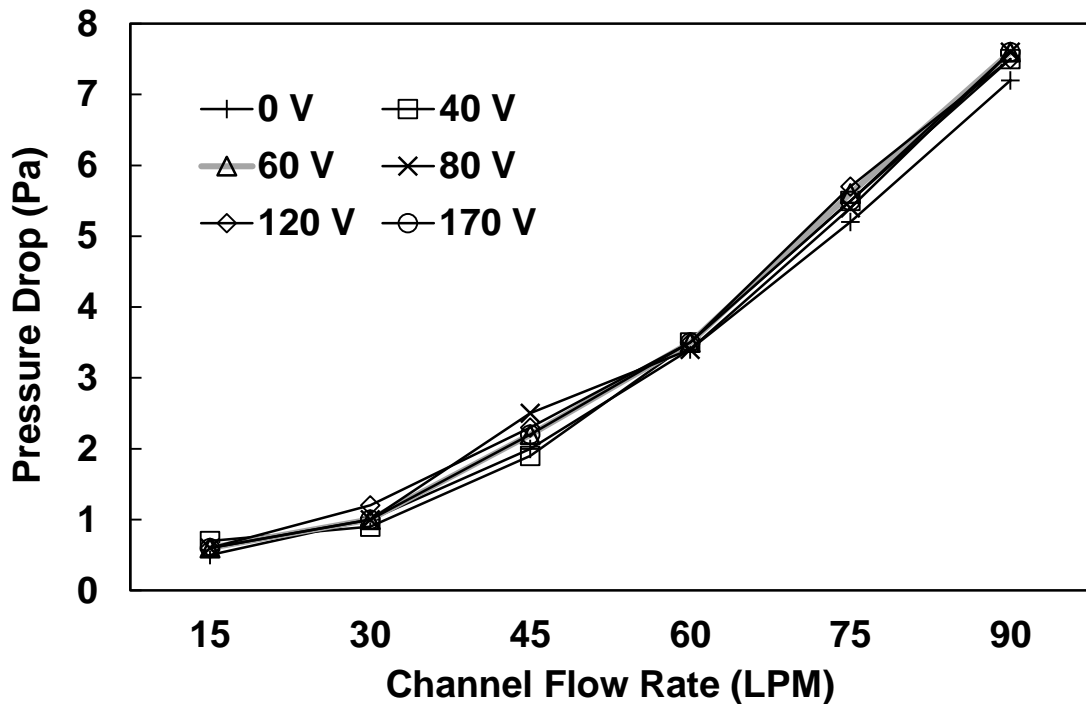
Figure 14. Pressure drop in the channel with the PE fans operating at different voltages.

Fig. 14 presents the pressure drop measured over the entire length of the channel when the PE fan was aligned at the front-end location. The location of the PE fan had an almost negligible impact on the pressure drop across the channel. In general, the pressure drop significantly increased with the channel flow rate. On the other hand, the excitation voltage of the PE fan did not significantly impact the pressure drop. Overall, the PE fan did not contribute significantly to the pressure drop across the channel compared to the channel flow. This can be a

significant benefit when considering using the PE fan as an aid-device to improve the convection heat transfer of channel flow. However, we have not tested the PE fan with multiple operating frequencies in the current study. Therefore, the effects of the operating frequency on the pressure drop are not apparent yet and should be examined in future studies.

CHAPTER 3

NUMERICAL STUDY

3.1 Simulation Setup

Numerical simulations were performed to uncover the underlying physics of the channel's heat transfer enhancement with the PE fan. The simulation domain reproduces the air channel of the experimental test section in which the heated surface and the PE fan are located. The channel's length is shortened to 140 mm in the simulation, excluding the upstream and downstream extensions, used to secure a fully-developed and stable channel flow in the experiment. A fully-developed flow condition with an average velocity of 3 m/s is provided at the channel's inlet to minimize any discrepancies from the experimental setup due to the channel's reduced length. The outlet of the channel is treated as the pressure outlet condition to prevent a reverse flow. At both inlet and outlet of the channel, the turbulent intensity and viscosity ratio are kept as 5% and 10, respectively. Among the three locations of the PE fan tested in the experiment, the case where the fan tip is aligned at the front-end of the heated surface is selected for further investigations in the simulation. The inlet air temperature is given as 297.15 K. The constant heat-flux condition of 4,370.6 W/m^2 is given to the heated surface as a thermal boundary condition. For simplified replication of the motion of the PE fan in the heat transfer channel, the user-defined function (UDF), embedded in the commercial CFD package of ANSYS Fluent, was used to realize the flapping motion of the PE fan over the heated surface in the channel. The flapping motion of the PE fan is defined with the sine wave, suggested by Ma et al. [23]:

$$y(\gamma, t) = \frac{D}{2} * \left(\frac{\gamma}{L_{PE}}\right)^2 * \sin(2\pi f t) \tag{17}$$

where y is the displacement at an arbitrary location, γ, along the PE fan from its rotational axis. D is the amplitude of PE fan, L_{PE} represents the effective lengths of the PE fan that adds L_b and L_p. f is the operating frequency of the PE fan.
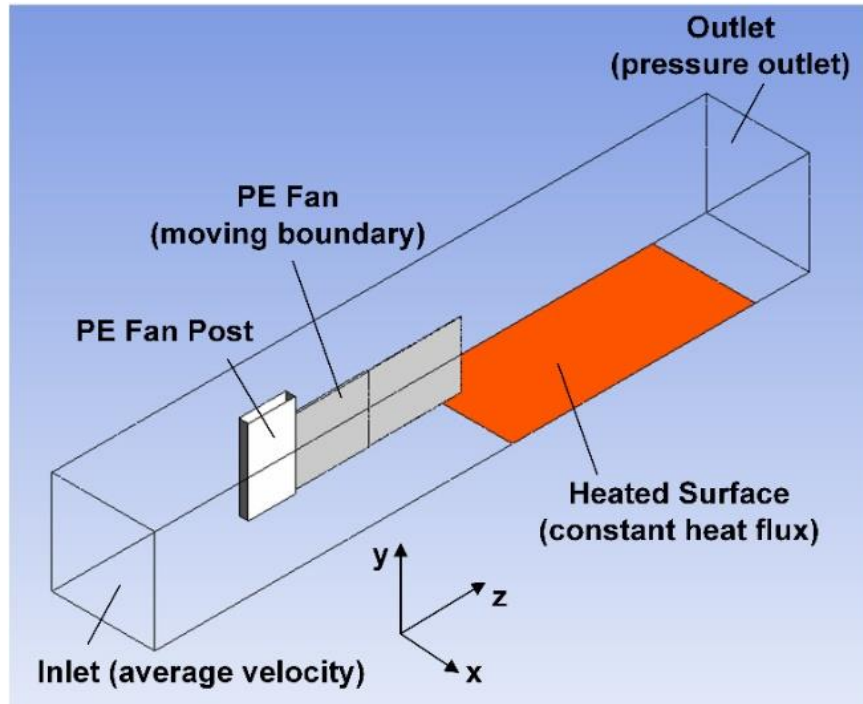
Figure 15. Domains and boundary conditions of the channel in the numerical study

The operating frequency of the PE fan used in the numerical study is 90.3 Hz. A single cycle of the PE fan operation was divided into 400 equal time steps. A small number of time steps per cycle leads to a large discretization error, while a large number of time steps per cycle increases computational cost. In the current study, 400 time steps per cycle (corresponding to a time step size of 2.76855×10^{-5} s) was selected as a compromise between the discretization error and computational cost. A simulation was run for a total of 10,000 time steps (25 oscillation cycles) until the solution reached the quasi-steady-state. All the physical walls, including the PE

fan surfaces in the channel, are treated as a no-slip boundary condition. The detailed illustrations

of the simulation domains and corresponding boundary conditions are provided in **Fig. 15**.

The pressure-based, transient solver is used in ANSYS Fluent to solve the three

governing equations of the compressible continuity, Navier-Stokes, and energy equations, shown

below:

$$\frac{\partial \rho}{\partial t} + \nabla \cdot (\rho \vec{v}) = 0 \tag{18}$$

$$\frac{\partial}{\partial t}(\rho \vec{v}) + \nabla \cdot (\rho \vec{v} \vec{v}) = -\nabla p + \nabla \cdot (\bar{\tau}) \tag{19}$$

$$\frac{\partial}{\partial t}(\rho E) + \nabla \cdot \left(\vec{v}(\rho E + p)\right) = \nabla \cdot \left(k_{eff} \nabla T + \left(\bar{\tau}_{eff} \cdot \vec{v}\right)\right) \tag{20}$$

where ρ, t, $\vec{v}$, p, T, $\bar{\tau}$, and k denote the density, time, velocity vector, pressure, temperature, stress

tensor, and thermal conductivity, respectively. The subscript *eff* represents the effective quantities

of associated turbulent properties. Herein, E represents the energy term, which includes the

enthalpy (h) and static and dynamic pressures as below:

$$E = h - \frac{P}{\rho} + \frac{v^2}{2} \tag{21}$$

The shear-stress transport (SST) k-ω [36,46] and the standard k-ε model [12] have been

widely known for providing high-fidelity results on resolving complex flow patterns around the

blade tips of PE fans. The transition SST model [47–49] is effective in investigating the flow

fields that have both the laminar and turbulent flow regimes existing together. More recent

studies [21,22,40] have proved that the renormalization group (RNG) k-ε model can effectively

characterize the generation and transport natures of vortex structures created by PE fans,

subjected to a channel flow condition. In the current study, understanding their transport

characteristics and impinging dynamics onto the heated surface is essential to reveal the

fundamental mechanism of convection heat transfer enhancement of the channel flow. Therefore,

the RNG k-ε model, expressed in the Eqs. (22) and (23), is used for capturing the turbulent viscosity generated by the PE fan in the current study.

$$\frac{\partial}{\partial t}(\rho k) + \nabla \cdot (\rho k \vec{v}) = \nabla.\left(\alpha_k \mu_{eff} \nabla k\right) + G_k - \rho \varepsilon \qquad (22)$$

$$\frac{\partial}{\partial t}(\rho \varepsilon) + \nabla \cdot (\rho \varepsilon \vec{v}) = \nabla.\left(\alpha_\varepsilon \mu_{eff} \nabla \varepsilon\right) + C_{1\varepsilon}\frac{\varepsilon}{k}G_k - C_{2\varepsilon}\rho\frac{\varepsilon^2}{k} - R_\varepsilon \qquad (23)$$

More details regarding the parameters included in Eqs. (22) and (23) can be found in the literature [50,51]. Multiple virtual planes in all x, y, and z directions of the fluid domain are created to observe the spatial distributions of various thermal and fluid properties, as shown in **Fig. 16**.
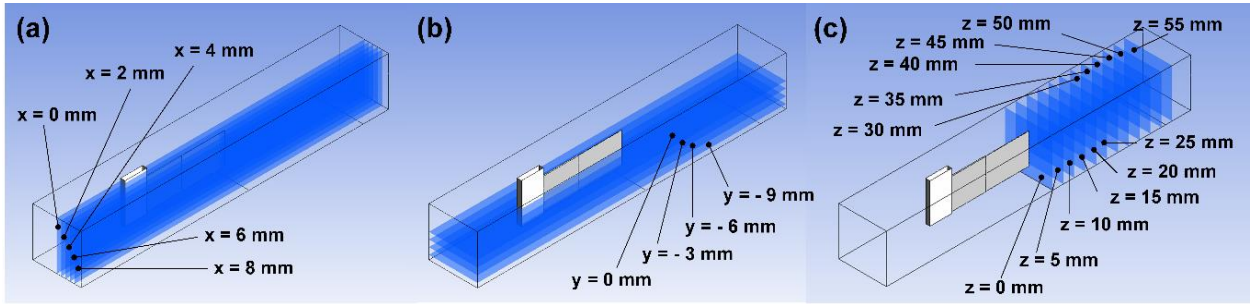
Figure 16. Virtual planes for observing numerical simulation results

3.2 Validation and Mesh Independence Study

Fig. 17 shows the mesh of the simulation domains used in the current study. The section views of the meshed domains on the planes of x = 0 and z = 0 are shown in **Fig. 17(b)** and **17(c)**, respectively. The meshing was done using the linear unstructured tetrahedron elements. The element cells near the fan tip experience significant deformations as the PE fan follows the vibrating motion with a large displacement. So the element structures around the fan tip were refined correctly to prevent any numerical divergence. Similarly, the areas of significant importance, such as the areas around the heated surface, were refined to improve computational accuracy. As mentioned earlier, the motion of the PE fan was realized using the UDF function

36

with eqs. (17). The UDF used to realize the motion of the PE fan is given in the Appendix 1.The dynamic meshing technique was used to realize the motion of the PE fan. Among the three methods available in Ansys Fluent (layering, smoothing, and remeshing), the spring-based smoothing and remeshing methods were implemented. In the spring-based smoothing method, the edges of each element are treated as interconnecting springs. When the edges experience deformations, the force on each elemental node varies proportionally to the displacement of the spring. If the smoothing method is only used, the elements near the fan tip get highly skewed due to the motion of the PE fan. These highly skewed elements can result in floating-point errors. Therefore, the remeshing method was also applied for the dynamic meshing at every time step to reduce floating-point errors.
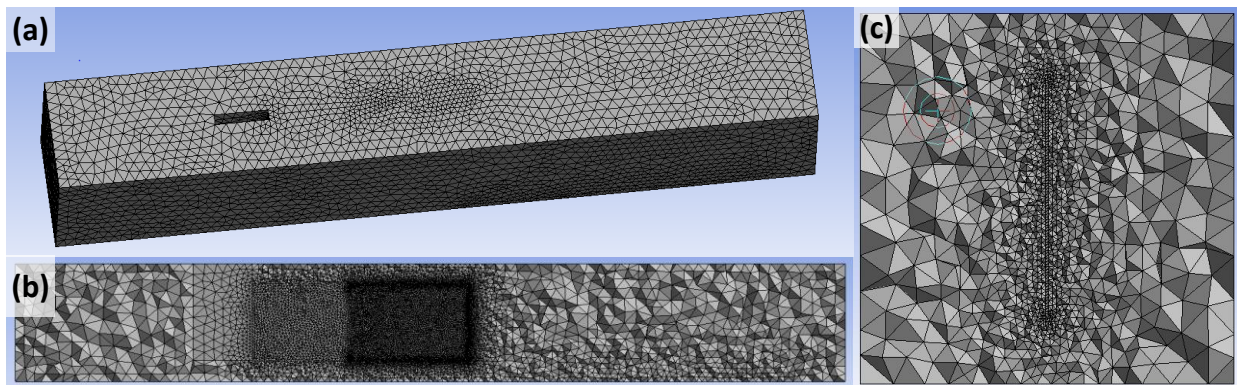
Figure 17. Mesh of the simulation domain (a) iso-metric view, (b) section view at the plane x = 0 mm, (c) section view at the plane z = 0 mm

The inlet and outlet temperatures of the computational study were obtained by conducting the mass-averaging on the static temperatures at the inlet and outlet of the channel, respectively. The average temperature of the heated surface was obtained by area-averaging the static temperatures of the heated surface. Then, the heat transfer coefficient at the specific time step was calculated using the LMTD method. The average heat transfer coefficient of the heated surface was obtained by time-averaging the heat transfer coefficient of all the time steps for a

single cycle of the PE fan after the simulation reached a quasi-steady-state. A mesh independence study was conducted to ensure the validity of the numerical methodology. For the study, the case with the channel velocity of 3 m/s and *D/W* of 0.5 was used. Three simulation cases with different numbers of total elements were created, and they were named Mesh-1, Mesh-2, and Mesh-3. The numbers of total elements of Mesh-1, 2, and 3 were 395,575, 505,509, and 602,068, respectively. The corresponding average heat transfer coefficients are summarized in **Table 5**. As a result, the average heat transfer coefficient of the heated surface started converging as the number of total elements reached around 500,000. Therefore, the total element number was kept around 500,000 for the simulation cases conducted in the numerical study.

Table 5. The results of mesh independence study

	Mesh-1	**Mesh-2**	**Mesh-3**
Number of Total Elements	395,575	505,509	602,068
Average Heat Transfer Coefficient (W/m²K)	55.4	64.2	64.6

The average heat transfer coefficients obtained from the numerical study were also compared against the experimental results to further validate the computational methodology. As a result, experimental and computational results showed good agreement on the average heat transfer coefficients of the heated surface at various channel velocities and PE fan's displacements. **Fig. 18(a)** compares the heat transfer coefficients at different channel flow velocities while keeping the PE fan's displacement as 11.8 mm (*D/W* = 0.53). Although the results at the low channel velocities of 0.5 and 1.0 m/s showed the differences of around 15 ~ 20% between the experiment and computation, the deviations started reducing significantly as the channel velocity increased above 1 m/s. Secondly, **Fig. 18(b)** compares the experimental and computational results obtained for different PE fan displacements at the fixed channel velocity of

3 m/s. As a result, the experiment and computation showed good agreement with the differences of less than 10% for all the conditions considered.
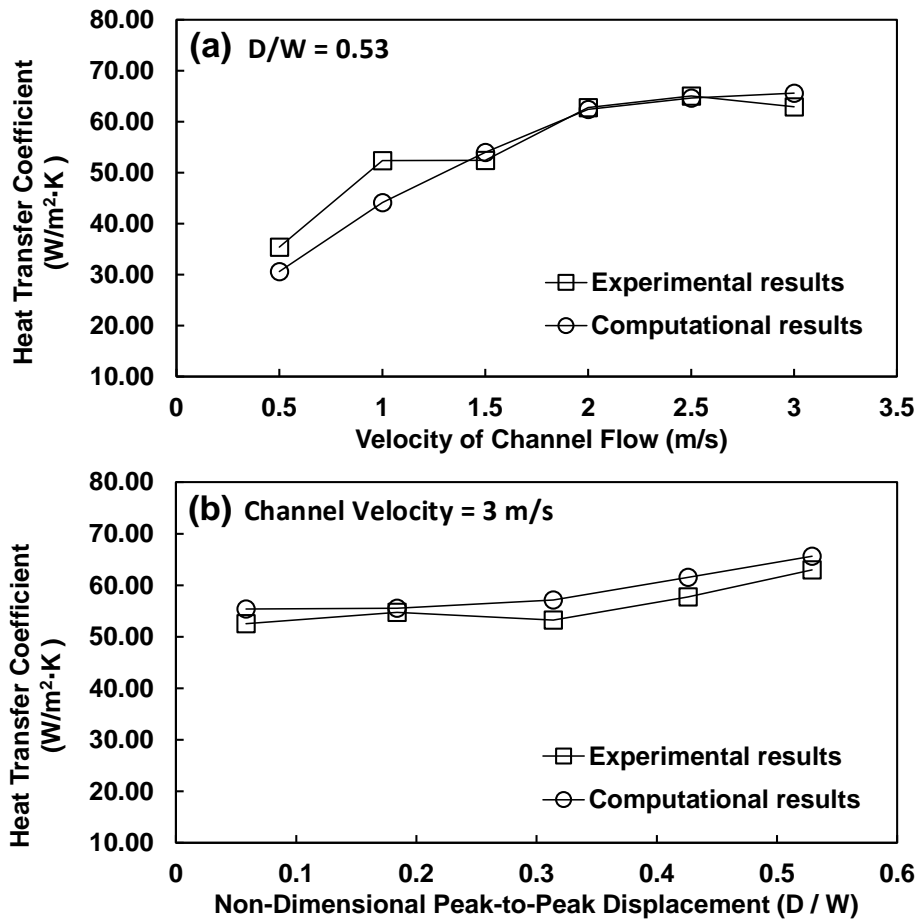
Figure 18. Validation of the numerical simulation

3.3 Results and Discussions

In order to obtain the fundamental understanding of the convection heat transfer enhancement by the PE fan in the channel flow, the current study focused on observing the formation and transport characteristics of vortex structures generated from the PE fan and their impinging dynamics onto the heated surface. In **Fig. 19**, the Q-criterion analysis, which configures a connected fluid region where the vorticity magnitude is greater than the strain-rate [52,53], was used to identify the vortex structures generated at different phases (ϕ) of the PE fan operation. The data was collected over the half-cycle of the PE fan operation after each cycle of

flow and heat transfer processes were assumed to reach the steady-state condition. At the phase of $\phi = 0$, the fan tip is positioned in the center of the channel moving towards the positive x-direction. It is seen that streamwise (positive z-direction) and wall-normal-wise (positive y-direction) vortices are generated from the three edges of the PE fan while they are sweeping the flow field across the channel flow. Then, the generated vortices are left behind the fan and carried downstream by the channel flow. When the vortices leave the edges of the fan, they get connected, forming a large closed-loop vortical structure (VS) that maintains its dynamic characteristics until it completely passes over the heated surface. While the vortical structures (VSs) transport downstream, they do not travel along the centerline; instead, they tilt to the two side walls of the channel following the directions of the fan at the moments when the VSs leave the fan edges. For example, if the VS is generated when the fan tip moves to the positive x-direction, it inclines to the positive x-direction while traveling downstream. Therefore, we can see that the VSs are aligned as a footstep formation along the channel. At the instantaneous time of $\phi = 0$, VS-1 is generated from the fan tip, and VS-2, 3, and 4 are being transported downstream.
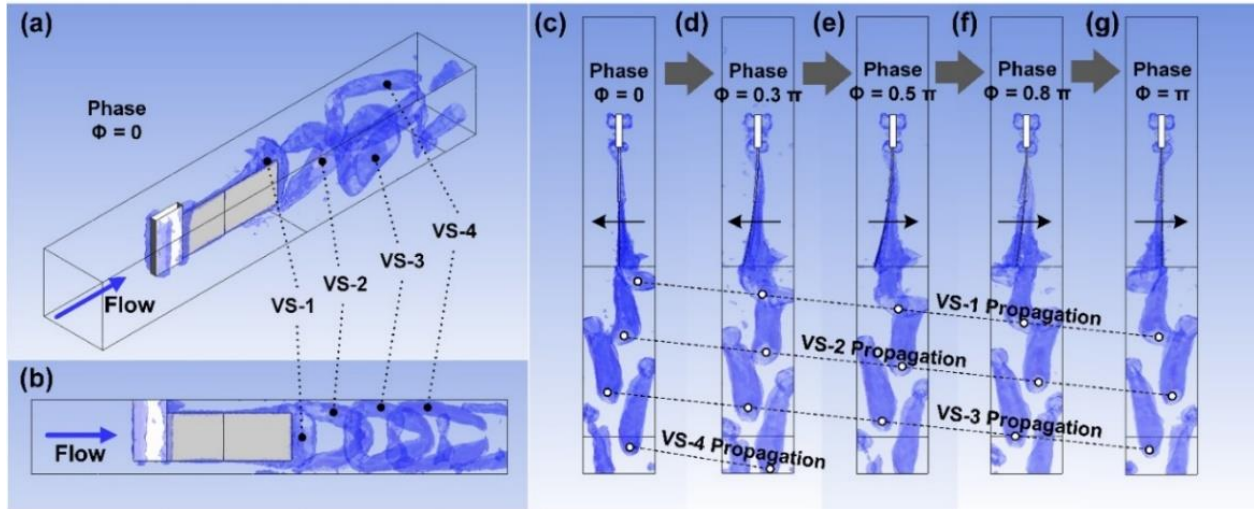
Figure 19. Visualizations of vortex formations with Q-criterion technique at different phases of the PE fan in the channel.
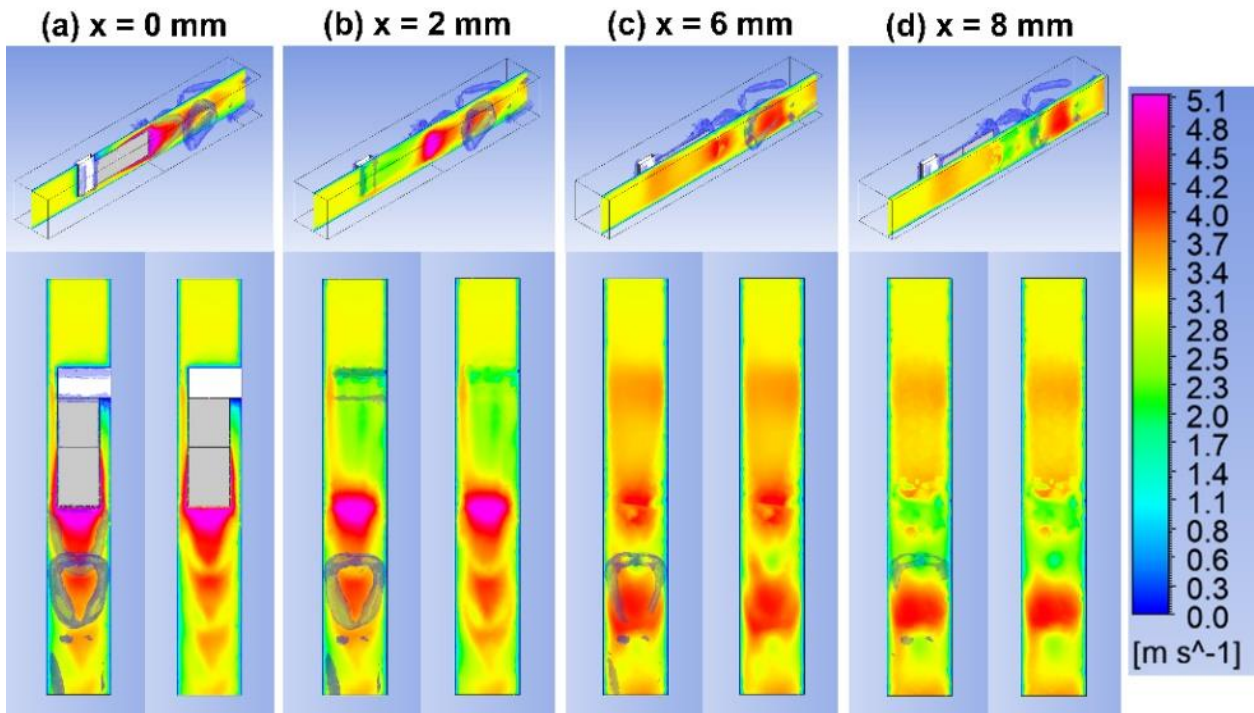
Figure 20. Velocity contours of different x-planes at the zero-phase operation
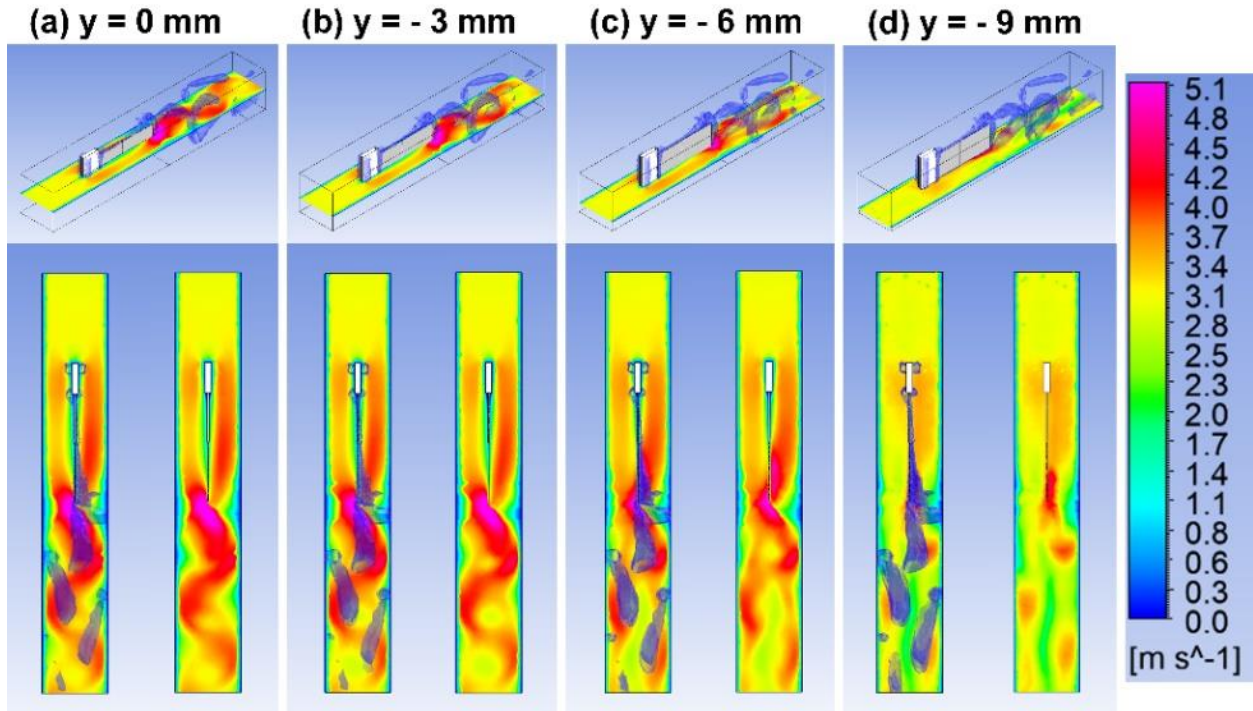
Figure 21. Velocity contours of different y-planes at the zero-phase operation

Figs. 20 and **21** show the velocity contours in the channel at different x and y planes at the phase of $\phi = 0$. The velocity contours clearly show that the zones made by the closed-loops of the VSs contain high momentum energy provided by the flapping motion of the PE fan. The areas within the VSs exhibit very high velocities compared to the average channel velocity, and they are collectively carried downstream while still being confined within the loops of the VSs. Therefore, it is evident that the PE fan plays the roles of 1) providing additional momentum energy to the channel for increasing the average channel velocity and 2) generating concentrated high momentum zones enclosed by the vortex rings that can intermittently impinge on the heated surface. These two major phenomena are assumed to be the direct effects caused by the PE fan for enhancing the convection heat transfer of the channel. However, as the flow moves downstream, the strength of the VSs is diminished, and the channel starts recovering the

upstream un-agitated conditions again. This phenomenon is also shown in **Fig. 19** with the

weakened VSs downstream of the channel. Hence, these observations indicate that the relative

location of the PE fan compared to the heated surface must be one of the essential factors in the

design of the heat transfer channel with the PE fan. **Fig. 22** shows the variations of the average

channel velocities at different phases of the PE fan along the channel. The velocities are non-

dimensionalized by the channel inlet average velocity, U_{in}. The average channel velocity

increases about 12% compared to the average inlet velocity immediately downstream of the fan

and gradually decreases as the flow further moves downstream. At the end of the heated surface,

the channel velocity almost recovers the inlet condition.
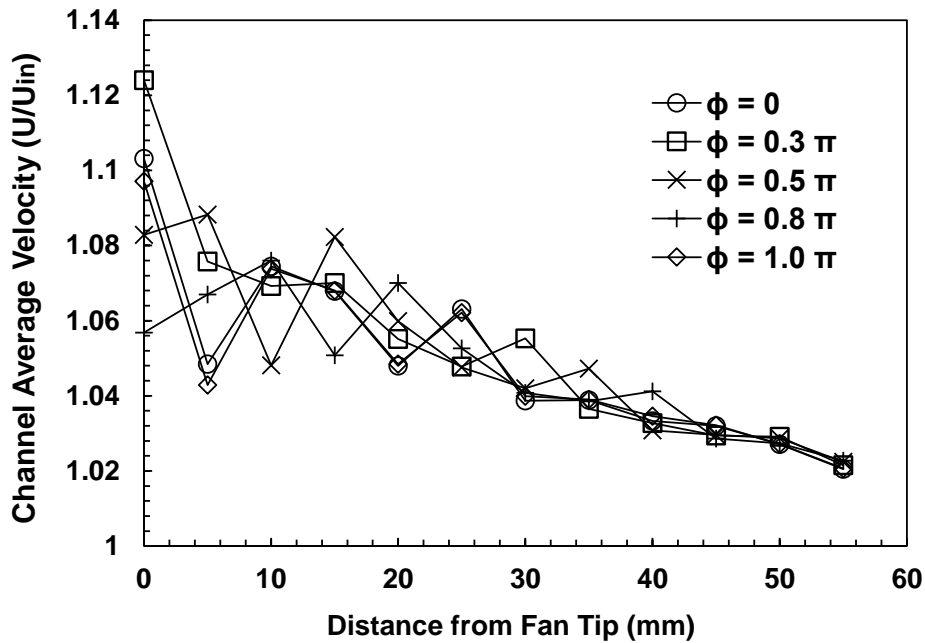
Figure 22. Non-dimensionalized channel average velocity at different distances from the fan
tip along the streamwise direction

Based on the observations made from **Figs. 19 ~ 22**, the PE fan significantly alters the

fluid dynamic characteristics of the channel flow generating the high-momentum zones within

the VSs, and they are assumed to be highly related to the enhancement of the channel convection

43

heat transfer. Therefore, revealing a physical link between the dynamics of the VSs and the thermal responses of the heated surface is a necessary next step that must be performed to obtain the fundamental understanding. In **Fig. 23**, the attempt has been made to overlap the VSs along with the local temperature responses of the heated surface. The VS is dissected into the sub-components of head, legs, and tail vortices for detailed explanations. The head is a u-shaped vortex at the front of the VS. The legs are two vortices horizontally aligned along the streamwise direction (z-direction) connecting the head and tail vortices. The tail is a single wall-normalwise (y-direction) vortex positioned at the trailing edge of the VS.
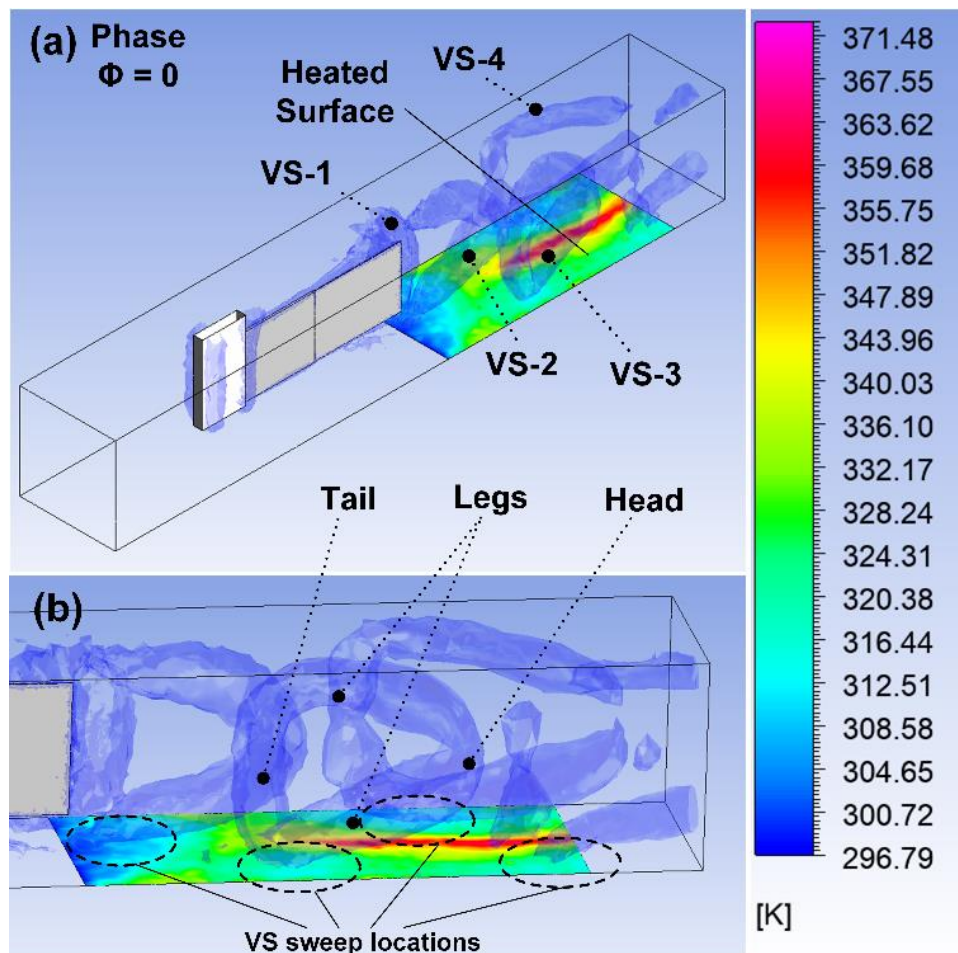
Figure 23. Visualizations of vortex structures over the heated surface with the PE fan at $\phi = 0$.

In **Fig. 23 (b)**, there are several locations where the VSs are in direct contact with the heated surface. At these locations, the VSs are sweeping the heated surface with direct contacts. The low-temperature zones of the heated surface are nicely aligned with these direct sweeping locations. The heated surface in the vicinity of the fan tip shows the lowest temperatures due to the direct flow impingements created by the PE fan. In **Fig. 24**, the footprints of the VSs are projected onto the heated surface to show the instantaneous responses of the temperature field at the different phases of the PE fan operation. At all the phases observed, the low-temperature zones are nicely aligned with the trailing edges of the VSs propagating downstream as the phase evolves. The sweeping traces of the low-temperature zones are well presented in **Fig. 24 (b)**. One notable thing is that there is a localized hot spot formed along the center area of the heated surface at which the effects of the VSs are not reached. This hot spot's temperature reaches around 370 K, whereas the lowest temperature areas of the heated surface are still maintained at around 297 K.
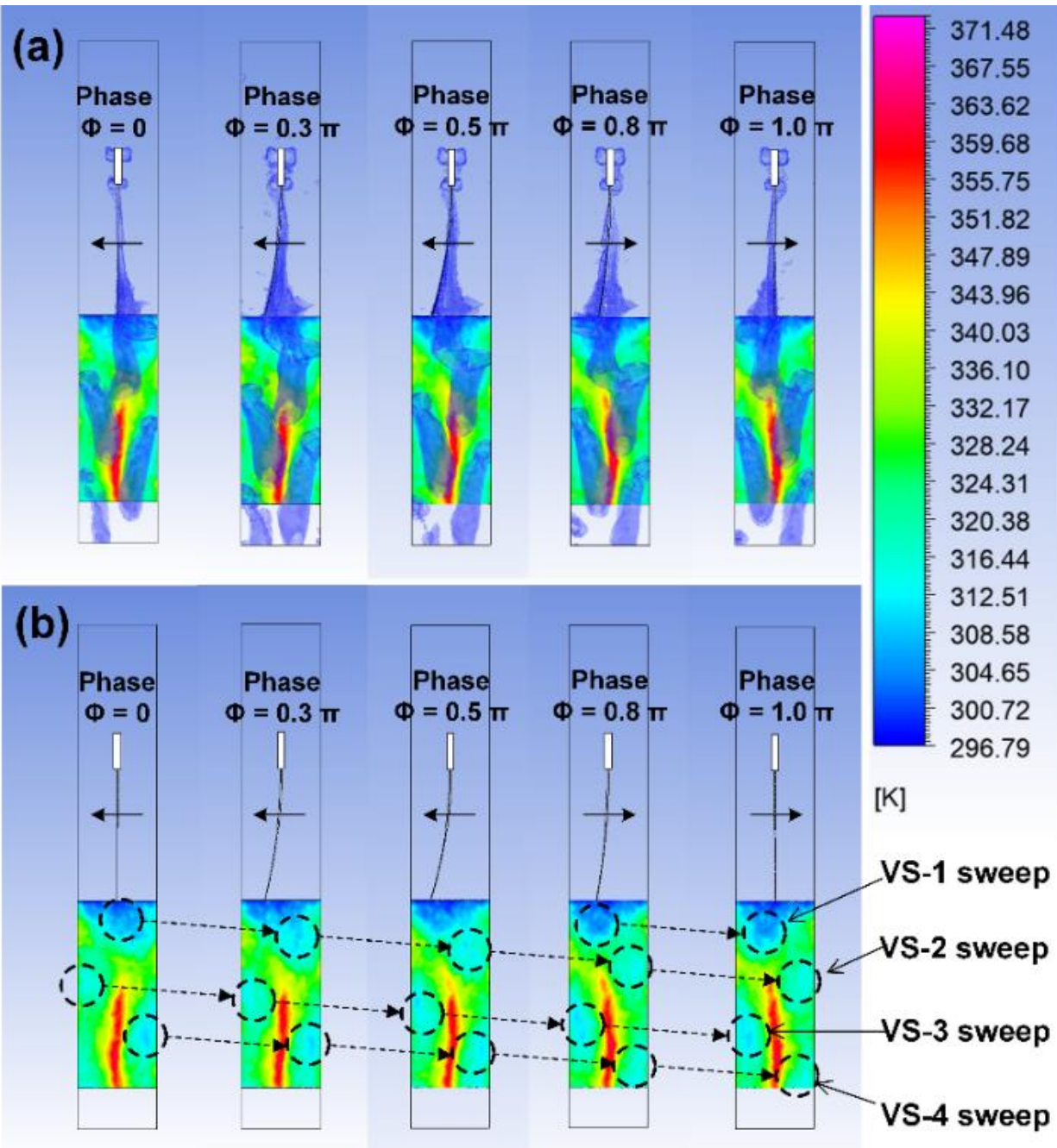
Figure 24. Observation of local temperature responses of the heated surface and the propagation of VSs at different phases of PE fan.
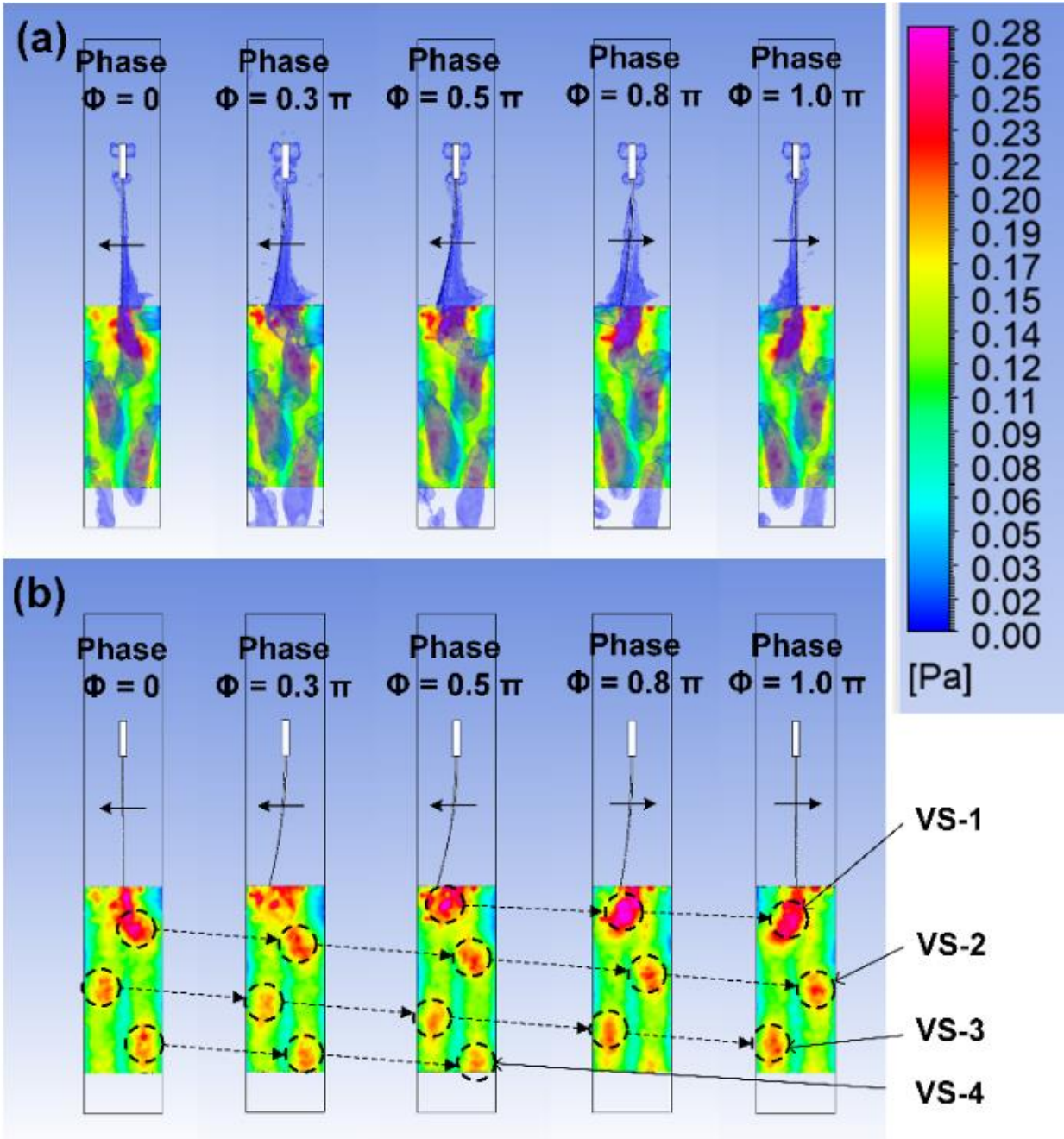
Figure 25. Observation on the propagation of vortex structures and surface shear stress at different phases of PE fan.

Finally, **Fig. 25** shows the distribution of shear stress of the heated surface to observe the dynamic relations between the convection heat transfer and surface shear stress. As expected, based on Chilton and Colburn's J-factor analogy [54,55], the areas with high shear-stresses are

well aligned with the areas with low temperatures over the heated surface within the footprints of the VSs in general. However, there is a slight offset that existed between the two areas within the footprints. Overall, the areas with high shear-stresses are formed ahead of the areas with low temperatures in the streamwise direction. From the comparison between **Fig 24. (b)** and **Fig. 25 (b)**, it can be seen that the low-temperature zones created by VS-4 still reside within the heated surface until the phase of $\phi = 1.0\,\pi$, whereas the corresponding high shear-stress zones complete its travel over the heated surface by the phase of $\phi = 0.5\,\pi$. As the surface shear stress is being one of the primary sources of the channel pressure drop, further investigations about the relationship between the dynamic responses of low temperature and high shear-stress of the heated surface may provide hints for achieving maximized heat transfer performance with minimized pressure drop penalty of the heat transfer channel system with the PE fan.

CHAPTER 4

CONCLUSIONS

This research work investigated the convection heat transfer performance of a PE fan placed in the air channel flow with a heated surface using experimental and numerical methods. In the experiment, the PE fan was placed horizontally along the streamwise direction of the channel, with the fan tip facing downwards. The rotational axis of the PE fan was vertically aligned with the heated surface. The impact of the PE fan on the convection heat transfer of the heated surface was studied by varying the displacement and relative location of the PE fan at various channel flow velocities. The operating frequency of the PE fan was fixed at 90.3 Hz. ANSYS Fluent was used to perform the numerical study for understanding the fundamental phenomena occurring on the fluid and thermal fields around the PE fan. The numerical study was explicitly focused on the case with the channel velocity of 3m/s and the maximum displacement of 11.8 mm. The key findings of the current study are highlighted below:

1. At Re_{cf} = 603, the lowest channel Reynolds number tested (equivalent channel flow rate of 15 LPM), the PE fan with its maximum peak-to-peak displacement of 11.8 mm enhanced the convection heat transfer rate of the heated surface by 102.2 % to the non-agitated channel condition. The tip of the PE fan was aligned to the leading edge of the heated surface (the front-end location).

2. When the channel Reynolds number was increased to its maximum value of 3,616 (equivalent channel flow rate of 90 LPM), the PE fan achieved the heat transfer enhancement of 33.2 % over the non-agitated channel at the same Reynolds number.

3. When the channel flow rate and excitation voltage were at their low levels, the location had a negligible impact on the heat transfer performance of the PE fan. In general, the PE fan either at the upstream or front-end location provided a better heat transfer performance than the one positioned at the center location regardless of the channel flow rates tested.

4. The effectiveness and Strouhal number analyses showed that there were critical operational conditions ($St_{cr} = 0.2$) below which the PE fan had a negative effect on the convection heat transfer enhancement of the channel.

5. The correlations between the heat transfer coefficient and total Reynolds number were generated that could be used to estimate the heat transfer performance of the PE fan in the channel for the given operational conditions.

6. Despite the superior cooling performances of the PE fan observed, its contributions to the channel pressure drop were negligible compared to those resulted by increasing the channel velocity.

7. As a result of the Q-criterion analysis, it was found that coherent vortical structures were created in the channel due to the operation of the PE fan. Based on the detailed observations of the generation and transport characteristics of the vortical structures, it was found that the direct impingement or sweeping of the vortical structures over the heated surface was mostly responsible for the heat transfer enhancement of the channel.

LIST OF REFERENCES

[1]   M. Toda, Theory of air flow generation by a resonant type PVF2 bimorph cantilever vibrator, Ferroelectrics. 22 (1978) 911–918. https://doi.org/10.1080/00150197908239445.

[2]   J.H. Yoo, J.I. Hong, W. Cao, Piezoelectric ceramic bimorph coupled to thin metal plate as cooling fan for electronic devices, Sensors and Actuators A: Physical. 79 (2000) 8–12. https://doi.org/10.1016/S0924-4247(99)00249-6.

[3]   T. Acikalin, S.V. Garimella, J. Petroski, Arvind Raman, Optimal design of miniature piezoelectric fans for cooling light emitting diodes, in: The Ninth Intersociety Conference on Thermal and Thermomechanical Phenomena In Electronic Systems (IEEE Cat. No.04CH37543), 2004: pp. 663-671 Vol.1. https://doi.org/10.1109/ITHERM.2004.1319239.

[4]   S.M. Wait, S. Basak, S.V. Garimella, A. Raman, Piezoelectric Fans Using Higher Flexural Modes for Electronics Cooling Applications, IEEE Transactions on Components and Packaging Technologies. 30 (2007) 119–128. https://doi.org/10.1109/TCAPT.2007.892084.

[5]   T. Lei, Z. Jing-zhou, T. Xiao-ming, Numerical investigation of convective heat transfer on a vertical surface due to resonating cantilever beam, International Journal of Thermal Sciences. 80 (2014) 93–107. https://doi.org/10.1016/j.ijthermalsci.2014.02.004.

[6]   M.K. Abdullah, N.C. Ismail, M.Z. Abdullah, M.A. Mujeebu, K.A. Ahmad, Z.M. Ripin, Effects of tip gap and amplitude of piezoelectric fans on the performance of heat sinks in microelectronic cooling, Heat Mass Transfer. 48 (2012) 893–901. https://doi.org/10.1007/s00231-011-0944-z.

[7]   S.-F. Liu, R.-T. Huang, W.-J. Sheu, C.-C. Wang, Heat transfer by a piezoelectric fan on a flat surface subject to the influence of horizontal/vertical arrangement, International Journal of Heat and Mass Transfer. 52 (2009) 2565–2570. https://doi.org/10.1016/j.ijheatmasstransfer.2009.01.013.

[8]   C.-N. Lin, Analysis of three-dimensional heat and fluid flow induced by piezoelectric fan, International Journal of Heat and Mass Transfer. 55 (2012) 3043–3053. https://doi.org/10.1016/j.ijheatmasstransfer.2012.02.017.

[9]   M. Kimber, S.V. Garimella, Measurement and prediction of the cooling characteristics of a generalized vibrating piezoelectric fan, International Journal of Heat and Mass Transfer. 52 (2009) 4470–4478. https://doi.org/10.1016/j.ijheatmasstransfer.2009.03.055.

[10]   N. Jeffers, K. Nolan, J. Stafford, B. Donnelly, High fidelity phase locked PIV measurements analysing the flow fields surrounding an oscillating piezoelectric fan, J. Phys.: Conf. Ser. 525 (2014) 012013. https://doi.org/10.1088/1742-6596/525/1/012013.

[11]   C.-N. Lin, Heat transfer enhancement analysis of a cylindrical surface by a piezoelectric fan, Applied Thermal Engineering. 50 (2013) 693–703. https://doi.org/10.1016/j.applthermaleng.2012.07.023.

[12]   M. Choi, C. Cierpka, Y.-H. Kim, Vortex formation by a vibrating cantilever, Journal of Fluids and Structures. 31 (2012) 67–78. https://doi.org/10.1016/j.jfluidstructs.2012.03.004.

[13]   A. Ihara, H. Watanabe, On the Flow Around Flexible Plates, Oscillating with Large Amplitude, Journal of Fluids and Structures. 8 (1994) 601–619. https://doi.org/10.1006/jfls.1994.1030.

[14]   Y.-H. Kim, S.T. Wereley, C.-H. Chun, Phase-resolved flow field produced by a vibrating cantilever plate between two endplates, Physics of Fluids. 16 (2003) 145–162. https://doi.org/10.1063/1.1630796.

[15]   Y.-H. Kim, C. Cierpka, S.T. Wereley, Flow field around a vibrating cantilever: coherent structure eduction by continuous wavelet transform and proper orthogonal decomposition, Journal of Fluid Mechanics. 669 (2011) 584–606. https://doi.org/10.1017/S0022112010005318.

[16]   A. Agarwal, K.P. Nolan, J. Stafford, N. Jeffers, Visualization of three-dimensional structures shed by an oscillating beam, Journal of Fluids and Structures. 70 (2017) 450–463. https://doi.org/10.1016/j.jfluidstructs.2017.02.013.

[17]   A. Eastman, J. Kiefer, M. Kimber, Thrust measurements and flow field analysis of a piezoelectrically actuated oscillating cantilever, Exp Fluids. 53 (2012) 1533–1543. https://doi.org/10.1007/s00348-012-1373-6.

[18]   A. Eastman, M.L. Kimber, Analysis of three-dimensional attributes and flow intake for an oscillating cantilever, Exp Fluids. 55 (2014) 1664. https://doi.org/10.1007/s00348-014-1664-1.

[19]   A. Eastman, M.L. Kimber, Aerodynamic damping of sidewall bounded oscillating cantilevers, Journal of Fluids and Structures. 51 (2014) 148–160. https://doi.org/10.1016/j.jfluidstructs.2014.07.016.

[20]   W.-J. Sheu, R.-T. Huang, C.-C. Wang, Influence of bonding glues on the vibration of piezoelectric fans, Sensors and Actuators A: Physical. 148 (2008) 115–121. https://doi.org/10.1016/j.sna.2008.06.028.

[21]   M.H. Oh, S.H. Park, Y.-H. Kim, M. Choi, 3D flow structure around a piezoelectrically oscillating flat plate, European Journal of Mechanics - B/Fluids. 67 (2018) 249–258. https://doi.org/10.1016/j.euromechflu.2017.09.002.

[22]   M.H. Oh, J. Seo, Y.-H. Kim, M. Choi, Endwall effects on 3D flow around a piezoelectric fan, European Journal of Mechanics - B/Fluids. 75 (2019) 339–351. https://doi.org/10.1016/j.euromechflu.2018.10.021.

[23]   H.K. Ma, H.C. Su, C.L. Liu, W.H. Ho, Investigation of a piezoelectric fan embedded in a heat sink, International Communications in Heat and Mass Transfer. 39 (2012) 603–609. https://doi.org/10.1016/j.icheatmasstransfer.2012.03.003.

[24]   C.-H. Huang, Y.-F. Chen, H. Ay, An inverse problem in determining the optimal position for piezoelectric fan with experimental verification, International Journal of Heat and Mass Transfer. 55 (2012) 5289–5301. https://doi.org/10.1016/j.ijheatmasstransfer.2012.05.037.

[25]   T. Açıkalın, A. Raman, S.V. Garimella, Two-dimensional streaming flows induced by resonating thin beams, The Journal of the Acoustical Society of America. 114 (2003) 1785–1795. https://doi.org/10.1121/1.1610453.

[26]   T. Açıkalın, S.V. Garimella, A. Raman, J. Petroski, Characterization and optimization of the thermal performance of miniature piezoelectric fans, International Journal of Heat and Fluid Flow. 28 (2007) 806–820. https://doi.org/10.1016/j.ijheatfluidflow.2006.10.003.

[27]   M.K. Abdullah, M.Z. Abdullah, M.V. Ramana, C.Y. Khor, K.A. Ahmad, M.A. Mujeebu, Y. Ooi, Z. Mohd Ripin, Numerical and experimental investigations on effect of fan height on the performance of piezoelectric fan in microelectronic cooling, International Communications in Heat and Mass Transfer. 36 (2009) 51–58. https://doi.org/10.1016/j.icheatmasstransfer.2008.08.017.

[28]   J. Petroski, M. Arik, M. Gursoy, Optimization of Piezoelectric Oscillating Fan-Cooled Heat Sinks for Electronics Cooling, IEEE Transactions on Components and Packaging Technologies. 33 (2010) 25–31. https://doi.org/10.1109/TCAPT.2009.2023859.

[29]   M. Kimber, K. Suzuki, N. Kitsunai, K. Seki, S.V. Garimella, Pressure and Flow Rate Performance of Piezoelectric Fans, IEEE Transactions on Components and Packaging Technologies. 32 (2009) 766–775. https://doi.org/10.1109/TCAPT.2008.2012169.

[30]   M. Kimber, S.V. Garimella, Cooling Performance of Arrays of Vibrating Cantilevers, J. Heat Transfer. 131 (2009). https://doi.org/10.1115/1.3153579.

[31]   T. Açikalin, S.V. Garimella, Analysis and Prediction of the Thermal Performance of Piezoelectrically Actuated Fans, Heat Transfer Engineering. 30 (2009) 487–498. https://doi.org/10.1080/01457630802529115.

[32]   S.F. Sufian, M.Z. Abdullah, J.J. Mohamed, Effect of synchronized piezoelectric fans on microelectronic cooling performance, International Communications in Heat and Mass Transfer. 43 (2013) 81–89. https://doi.org/10.1016/j.icheatmasstransfer.2013.02.013.

[33]   T. Acikalin, S.M. Wait, S.V. Garimella, A. Raman, Experimental Investigation of the Thermal Performance of Piezoelectric Fans, Heat Transfer Engineering. 25 (2004) 4–14. https://doi.org/10.1080/01457630490248223.

[34]   L.A. Florio, A. Harnoy, Use of a vibrating plate to enhance natural convection cooling of a discrete heat source in a vertical channel, Applied Thermal Engineering. 27 (2007) 2276–2293. https://doi.org/10.1016/j.applthermaleng.2007.01.023.

[35]   C.-N. Lin, Enhanced heat transfer performance of cylindrical surface by piezoelectric fan under forced convection conditions, International Journal of Heat and Mass Transfer. 60 (2013) 296–308. https://doi.org/10.1016/j.ijheatmasstransfer.2013.01.034.

[36]   X.-J. Li, J. Zhang, X. Tan, Convective heat transfer on a flat surface induced by a vertically-oriented piezoelectric fan in the presence of cross flow, Heat Mass Transfer. 53 (2017) 2745–2768. https://doi.org/10.1007/s00231-017-2019-2.

[37]   X.-J. Li, J. Zhang, X. Tan, An investigation on convective heat transfer performance around piezoelectric fan vibration envelope in a forced channel flow, International Journal of Heat and Mass Transfer. 126 (2018) 48–65. https://doi.org/10.1016/j.ijheatmasstransfer.2018.06.021.

[38]   T.-M. Jeng, C.-H. Liu, Moving-orientation and position effects of the piezoelectric fan on thermal characteristics of the heat sink partially filled in a channel with axial flow, International Journal of Heat and Mass Transfer. 85 (2015) 950–964. https://doi.org/10.1016/j.ijheatmasstransfer.2015.02.053.

[39]   S. Dey, D. Chakrborty, Enhancement of convective cooling using oscillating fins, International Communications in Heat and Mass Transfer. 36 (2009) 508–512. https://doi.org/10.1016/j.icheatmasstransfer.2009.01.018.

[40]   S.H. Park, M.H. Oh, Y.-H. Kim, M. Choi, Effects of freestream on piezoelectric fan performance, Journal of Fluids and Structures. 87 (2019) 302–318. https://doi.org/10.1016/j.jfluidstructs.2019.04.007.

[41]   J.P. Holman, Heat transfer, McGraw-Hill, New York; London, 1997.

[42]   T. Yeom, T.W. Simon, L. Huang, M.T. North, T. Cui, Piezoelectric translational agitation for enhancing forced-convection channel-flow heat transfer, International Journal of Heat and Mass Transfer. 55 (2012) 7398–7409. https://doi.org/10.1016/j.ijheatmasstransfer.2012.07.019.

[43]   T. Yeom, T.W. Simon, M. North, T. Cui, High-frequency translational agitation with micro pin-fin surfaces for enhancing heat transfer of forced convection, International Journal of Heat and Mass Transfer. 94 (2016) 354–365. https://doi.org/10.1016/j.ijheatmasstransfer.2015.11.054.

[44]   X.-J. Li, J. Zhang, X. Tan, Effects of piezoelectric fan on overall performance of air-based micro pin-fin heat sink, International Journal of Thermal Sciences. 126 (2018) 1–12. https://doi.org/10.1016/j.ijthermalsci.2017.12.018.

[45]   G.R. Iversen, M. Gergen, Statistics: The Conceptual Approach, Springer-Verlag, New York, 1997. https://doi.org/10.1007/978-1-4612-2244-6.

[46]   M.K. Abdullah, N.C. Ismail, M. Abdul Mujeebu, M.Z. Abdullah, K.A. Ahmad, M. Husaini, M.N.A. Hamid, Optimum tip gap and orientation of multi-piezofan for heat transfer enhancement of finned heat sink in microelectronic cooling, International Journal of Heat and Mass Transfer. 55 (2012) 5514–5525. https://doi.org/10.1016/j.ijheatmasstransfer.2012.05.024.

[47]   S. Bhattacharyya, S. Das, H. Chattopadhyay, Thermohydraulic characteristics and entropy analysis of a novel clockwise and anti-clockwise twisted sinusoidal wavy micro-channel under pulsating inlet condition, The European Physical Journal Applied Physics. 92 (2020) 20903. https://doi.org/10.1051/epjap/2020200176.

[48]   H. Chattopadhyay, T. Pal, D. Mandal, Flow and Heat Transfer due to Impinging Annular Jet, International Journal of Fluid Mechanics Research. 46 (2018). https://doi.org/10.1615/InterJFluidMechRes.2018018422.

[49]   H. Chattopadhyay, S.C. Murmu, Effect of inlet turbulence intensity on transport phenomena over bluff bodies, FMR. 47 (2020). https://doi.org/10.1615/InterJFluidMechRes.2020034333.

[50]   V. Yakhot, S.A. Orszag, Renormalization group analysis of turbulence. I. Basic theory, J Sci Comput. 1 (1986) 3–51. https://doi.org/10.1007/BF01061452.

[51]   D.N.A. G. C. Papageorgakis, Comparison of linear and nonlinear RNG-based k-epsilon models for incompressible turbulent flows, Numerical Heat Transfer, Part B: Fundamentals. 35 (1999) 1–22. https://doi.org/10.1080/104077999275983.

[52]   J.C. Hunt, A.A. Wray, P. Moin, Eddies, streams, and convergence zones in turbulent flows, (1988).

[53]   Y. Dubief, F. Delcayre, On coherent-vortex identification in turbulence, Journal of Turbulence. 1 (2000) N11. https://doi.org/10.1088/1468-5248/1/1/011.

[54]   A.P. Colburn, A method of correlating forced convection heat transfer data and a comparison with fluid friction, Trans Am Inst Chem Engrs. 29 (1993) 174–210.

[55]   T.H. Chilton, A.P. Colburn, Mass transfer (absorption) coefficients prediction from data on heat transfer and fluid friction, Industrial & Engineering Chemistry. 26 (1934) 1183–1187.

APPENDIX

Appendix 1

UDF to realize the motion of Piezoelectric Fan

```c
#include"udf.h"
#include "math.h"
#define pi 3.141592645
DEFINE_GRID_MOTION (motion, domain, dt, time, dtime)
{
Thread *tf = DT_THREAD(dt);
face_t f;
Node *v;
real NV_VEC(axis);
real displ;
int n;
real NV_VEC (origin);
real NV_VEC (omega);
real amp;        /* define amplitude of the PE fan as real number */
real freq;       /* define frequency of the PE fan as real number */
real omegas;     /* define omega =2*pi*f */
real length;     /* length of fan in mm */
amp = 5.55;      /* unit mm, mean to peak amplitude */
freq = 90.3;     /* hz */
omegas = 2 * 3.141592 * freq;
length = 36.5;   /* mm */
displ= amp*1000/length/length * omegas * cos(omegas*time);       /* grid displacement*/
NV_D(axis, =, 1.0, 0.0, 0.0);            /*define the axis of rotation */
```

```
NV_D (origin, =, 0.0, 0.0, 0.0);          /*define origin */

begin_f_loop(f,tf)

{

f_node_loop(f,tf,n)

{

v = F_NODE(f,tf,n);   /* update node if the current node has not been previously visited when
looping through previous faces */

if ( NODE_POS_NEED_UPDATE (v))        /* indicate that node position has been update so
that it's not updated more than once */

{

NODE_POS_UPDATED(v);

NV_V_VS(NODE_COORD(v), =, NODE_COORD(v), +, axis,*,displ*NODE_Z(v)*
NODE_Z(v)*dtime);          /* update the position of node with new position according to
displacement of PE fan */

}

}

}

end_f_loop(f,tf);

}
```

VITA

Janak Tiwari, born and raised in Nepal, came to University of Mississippi to pursue Master in Engineering Science in Department of Mechanical Engineering. He completed his Bachelor in Mechanical Engineering from Anna Univeristy, India. Prior to joining the University of Mississppi, he worked as a Mechanical Engineer for two years in Nepal. During his master study, he researched on enhancement of convection heat transfer in rectangular channel using piezoelectric fans. After graduating from OleMiss, he is planning to pursue doctorate at the University of Utah.